

A Single-Ion Magnet Building Block Strategy Toward Dy₂ Single-Molecule Magnets with Enhanced Magnetic Performance

Dong Shao,^{†a,d} Prem Prakash Sahu,^{†c} Wan-Jie Tang,^a Yang-Lu Zhang,^a Yue Zhou,^a Fang-Xue Xu,^d Xiao-Qin Wei,^{*b} Zhengfang Tian,^a Saurabh Kumar Singh^{*c} and Xin-Yi Wang ^{*d}

^a Hubei Key Laboratory of Processing and Application of Catalytic Materials, College of Chemistry and Chemical Engineering, Huanggang Normal University, Huanggang 438000, P. R. China

^b Department of Material Science and Engineering, Shanxi Province Collaborative Innovation Center for Light Materials Modification and Application, Jinzhong University, Jinzhong, 030619, P. R. China.

^c Department of Chemistry, Indian Institute of Technology Hyderabad, Kandi-502285, Sangareddy, Telangana, India

^d State Key Laboratory of Coordination Chemistry, Collaborative Innovation Center of Advanced Microstructures, School of Chemistry and Chemical Engineering, Nanjing University, Nanjing, 210023, P. R. China.

Correspondence and requests for materials should be addressed to

Email: wangxy66@nju.edu.cn (X. Y. W.) or sksingh@chy.iith.ac.in (S. K. S.)

Table of Contents

EXPERIMENTAL SECTION.....	5
COMPUTATIONAL DETAILS.....	6
Figure S1. The asymmetric units of 2 (a) and 3 (c), and the complete molecule structures of 2 (b) and 3 (d) in ellipses & sticks mode.	8
Table S1. Selected bond lengths (\AA) and bond angles ($^{\circ}$) for 2.	9
Table S2. Selected bond lengths (\AA) and bond angles ($^{\circ}$) for 3.	10
Table S3. Continuous Shape Measure (CSM) analysis for eight-coordinated Dy^{3+} ions in 2 and 3 ...	11
Figure S2. A portion of one-dimensional coordination chain structure of 2 along two main crystallographic axes: the a axis (a) and the b axis (b).	12
Figure S3. A portion of one-dimensional coordination chain structure of 3 along two main crystallographic axes: the b axis (a) and the c axis (b).	13
Figure S4. Comparison of the experimental PXRD patterns of 2 and 3 with the simulated patterns from single crystal structure. The calculated patterns were generated from Mercury using the CIF of the crystal structure.....	14
Figure S5. TGA curves of 2 and 3 measured under the Argon atmosphere upon the continuous heating with the $10 \text{ } ^{\circ}\text{C}\cdot\text{min}^{-1}$ rate.....	15
Figure S6. IR spectra of complexes 1 , 2 and 3	15
Figure S7. Variable-field magnetization at 2 K for 2 (up) and 3 (down).	16
Figure S8. Temperature dependence of the in-phase (χ') and out-of-phase (χ'') part of the ac susceptibilities measured under zero dc field for 2	17
Figure S9. Temperature dependence of the in-phase (χ') and out-of-phase (χ'') part of the ac susceptibilities measured under zero dc field for 3	18
Table S4. Relaxation fitting parameters from the least-square fitting of the Cole-Cole plots of compound 2 under zero dc filed according to the generalized Debye model.	19
Table S5. Relaxation fitting parameters from the least-square fitting of the Cole-Cole plots of compound 3 under zero dc filed according to the generalized Debye model.	20
Table S6. RASSI-SO computed low-lying 21 spin-free sextet states and the spin-orbit coupled (Kramer doublets) for Dy center in monomer complex 1. All the values are reported here in cm^{-1} . The values in red colour are for the spin-free sextet states while the values in the blue colour are for the spin-orbit coupled states.	21
Table S7. RASSI-SO computed low-lying 21 spin-free sextet states and the spin-orbit coupled (Kramer doublets) for Dy@1 center in dimer complex 2. All the values are reported here in cm^{-1} . The values in red colour are for the spin-free sextet states while the values in the blue colour are for the spin-orbit coupled states.	22
Table S8. RASSI-SO computed low-lying 21 spin-free sextet states and the spin-orbit coupled (Kramer doublets) for Dy@2 center in dimer complex 2. All the values are reported here in cm^{-1} . The values in red colour are for the spin-free sextet states while the values in the blue colour are for the spin-orbit coupled states.	23

Table S9. RASSI-SO computed low-lying 21 spin-free sextet states and the spin-orbit coupled (Kramer doublets) for Dy@1 center in dimer complex 3. All the values are reported here in cm ⁻¹ . The values in red colour are for the spin-free sextet states while the values in the blue colour are for the spin-orbit coupled states.	24
Table S10. RASSI-SO computed low-lying 21 spin-free sextet states and the spin-orbit coupled (Kramer doublets) for Dy@2 center in dimer complex 3. All the values are reported here in cm ⁻¹ . The values in red colour are for the spin-free sextet states while the values in the blue colour are for the spin-orbit coupled states.	25
Table S11. SINGLE_ANISO computed g-tensors, the angle of deviation from ground state g_{zz} orientation, and relative energies of eight low lying Kramers' doublets for Dy center in monomer complex 1.	26
Table S12. SINGLE_ANISO computed g-tensors, the angle of deviation from ground state g_{zz} orientation, and relative energies of eight low lying Kramers' doublets for Dy@1 and Dy@2 centers in dimer complex 2.	26
Table S13. SINGLE_ANISO computed g-tensors, the angle of deviation from ground state g_{zz} orientation, and relative energies of eight low lying Kramers' doublets for Dy@1 and Dy@2 centers in dimer complex 3.	27
Table S14. SINGLE_ANISO computed crystal field parameters for Dy center in monomer complex 1. The major dominating values are kept in bold.	28
Table S15. SINGLE_ANISO computed crystal field parameters for Dy@1 and Dy@2 centers in both dimer complexes 2 and 3 respectively. The major dominating values are kept in bold.	29
Table S16. SINGLE_ANISO computed wave function decomposition analysis for Dy center in monomer complex 1. The major dominating values are kept in bold.	30
Table S17. SINGLE_ANISO computed wave function decomposition analysis for Dy@1 and Dy@2 centers in dimeric complex 2. The major dominating values are kept in bold.	31
Table S18. SINGLE_ANISO computed wave function decomposition analysis for Dy@1 and Dy@2 centers in dimeric complex 3. The major dominating values are kept in bold.	32
Figure S10. Ab initio computed magnetic relaxation pathway for the (a) Dy center in monomer complex 1; (b) Dy@1 and (c) Dy@2 centers in dimer complex 2; and (d) Dy@1 and Dy@2 centers in dimer complex 3 respectively. The grey horizontal bars indicate the KDs as magnetic moments' function. The blue, red, and green arrows represent the possible QTM/TA-QTM, Orbach, and Raman relaxation pathways.	33
Figure S11. CASSCF computed LoProp charges on the first coordinating atoms of Dy centers in (a) monomeric complex 1; (b) dimeric complex 2, and (c) dimeric complex 3 respectively.	34
Figure S12. Thermal dependence of the molecular magnetic susceptibility for (a) monomer complex 1; (b) dimer complex 2; (c) dimer complex 3. The grey diamond boxes are the experimental values, while the solid red lines represent the POLY_ANISO simulated data. NOTE: We have increased the simulated data by 4% to meet the experimental values in 2 and 3 respectively.	35
Figure S13. Magnetization at 2K for (a) dimer complex 2; (b) dimer complex 3 respectively. Solid blue lines represent the POLY_ANISO simulated data. NOTE: We have increased the simulated data by 4% to meet the experimental values.	36
Table S19. Exchange and dipolar interaction obtained from the POLY_ANISO simulation from the best fit using the Lines model for complexes 2 and 3.	37

Table S20. Energies of the low-lying non-Kramers' exchange doublets along with g_{zz} and tunneling gap obtained from POLY_ANISO simulation of complex 2.....	37
Table S21. Energies of the low-lying non-Kramers' exchange doublets along with g_{zz} and tunneling gap obtained from POLY_ANISO simulation of complex 3.....	38
Table S22. BS-DFT computed energies of high-spin and broken-symmetry solution of Gd analogue of complex 1 using $H=-JS_1S_2$ formalism. All J values are provided in cm^{-1}	38
Figure S14. Dimeric structure obtained from the crystal structure of complex 1 to compute the intermolecular exchange interaction.....	39
Table S23. Basis functions used in ab initio CASSCF calculations using MOLCAS code.	39
Table S24. Hydrogen optimized cartesian coordinates of complexes 1-3.	40
References	46

EXPERIMENTAL SECTION

Physical measurements.

Infrared spectra (IR) data were measured on KBr pellets using a Nexus 870 FT-IR spectrometer in the range of 4000-400 cm⁻¹. Elemental analyses of C, H, and N were performed at an Elementar Vario MICRO analyzer. Powder X-ray diffraction data (PXRD) were recorded on a Bruker D8 Advance diffractometer with Cu K α X-ray source ($\lambda = 1.54056 \text{ \AA}$) operated at 40 kV and 40 mA. Thermal gravimetric analysis (TGA) was measured in Al₂O₃ crucibles using a PerkinElmer Thermal Analysis in the temperature range of 30-800 °C under an argon atmosphere. Magnetic measurements from 1.8 to 300 K with applied direct current (dc) field up to 7 T were performed using a Quantum Design SQUID VSM magnetometer on the crushed samples from the single crystals of the compound. Alternative current (ac) magnetic susceptibility data were collected in a zero-dc field in the temperature range of 2-30 K, under an ac field of 2 Oe, oscillating at frequencies in the range of 1-1000 Hz. All magnetic data were corrected for the diamagnetic contributions of the sample holder and of core diamagnetism of the sample using Pascal's constants.

X-ray Crystallography.

Single crystal X-ray diffraction data were collected on a Bruker D8 QUEST diffractometer with a PHOTON III area detector (Mo-K α radiation, $\lambda = 0.71073 \text{ \AA}$, Bruker Ius 3.0) at 153 K. The APEX III program was used to determine the unit cell parameters and for data collection. The data were integrated and corrected for Lorentz and polarization effects using SAINT.^{S1} Absorption corrections were applied with SADABS.^{S2} The structures were solved by direct methods and refined by full-matrix least-squares method on F^2 using the SHELXTL^{S3} crystallographic software package integrated in Olex 2.^{S4} All the non-hydrogen atoms were refined anisotropically. Hydrogen atoms of the organic ligands were refined as riding on the corresponding non-hydrogen atoms. Additional details of the data collections and structural refinement parameters for complexes **2** and **3** are provided in Table 1. Selected bond lengths and angles of **2** and **3** were listed in Table S3. CCDC 2160454 and 2160455 are the supplementary crystallographic data for this paper. They can be obtained freely from the Cambridge Crystallographic Data Centre via www.ccdc.cam.ac.uk/data_request/cif.

COMPUTATIONAL DETAILS

All the analyses were performed on the X-ray crystal structures for complexes **1** and **2**, while for complex **3**, a truncated model was used to reduce the computational cost, where the terminal pyridine group of the bridging bpmo ligand was replaced with –H atom. The position of the hydrogens in complexes **1** and **2** and in the truncated model for complex **3** were optimized using ORCA/5.0.2 code^{S5}, employing BP86^{S6-S7} level of theory and def2-SVP^{S8-S9} basis set (see ESI for the optimized coordinates).

All the multi-reference calculations were performed using MOLCAS 8.2 code.^{S10} For calculations of spin-Hamiltonian parameters in Complete active space self-consistent field (CASSCF)^{S11} framework, an active space of CAS(9,7), i.e., nine active electrons in the seven active f-orbitals of Dy^{III} ion, was considered for all the monomer and dimer complexes. Here we have employed basis set for ANO-RCC library (see Table S23 for detailed basis set contraction scheme).^{S12-S13} To speed up the calculations, the two-electron integrals were computed using the Resolution of Identity Cholesky decomposition (RICD) approximation.^{S14} The single-ion properties of Dy^{III} ion in complex **1** was proceeded normally, but for dimeric complexes **2** and **3**, the other paramagnetic ion in the respective complexes was replaced with the diamagnetic Lu^{III} analogue. The Dy^{III} ion has 4f⁹ configuration and possesses a ⁶H_{15/2} ground state. Using the active space comprised of CAS(9,7), here we have computed 21 spin-free sextet states for all the complexes, and opted not to compute the other higher excited states, as the 21 roots is significant enough in describing the magnetic properties. The computed spin-free states for each Dy^{III} centers were subsequently mixed using a spin-orbit restricted active space spin-interaction (SO-RASSI) to compute the spin-orbit states.^{S15} These computed spin-orbit states were taken to the SINGLE_ANISO module^{S16} to extract the g-values, crystal field parameters, transition magnetic moments, magnetic susceptibility, and magnetization of individual Dy^{III} ion in all the complexes (monomeric **1**, and dimeric **2**, & **3**). The computed relative energies of the spin-free states, spin-orbit states, and the g-values are provided here in the Supporting Information.

Also, to confirm the nature of the magnetic interaction in complex **1**, we took the monomeric crystal structure and expanded it into a dimer. Calculations were performed on the isotropic Gd(III)-Gd(III) dinuclear complex, and the *J* values were further scaled for Dy(III) by a factor of 49/25 as mentioned earlier.^{S17} Our computed SH parameters nicely reproduce the static d.c. magnetic properties except for the very low-temperature ferromagnetic behaviour.

The sharp increase in $\chi_M T$ at very low-temperature in complex **1** arises from the weak intermolecular ferromagnetic interaction and this is supported by our DFT calculations.

Lastly using POLY_ANISO module,^{S18-S20} dc magnetic properties were simulated to extract the magnetic exchange interaction (dipolar + exchange contribution) between the Dy^{III} centers in dimeric complexes **2** and **3** respectively.

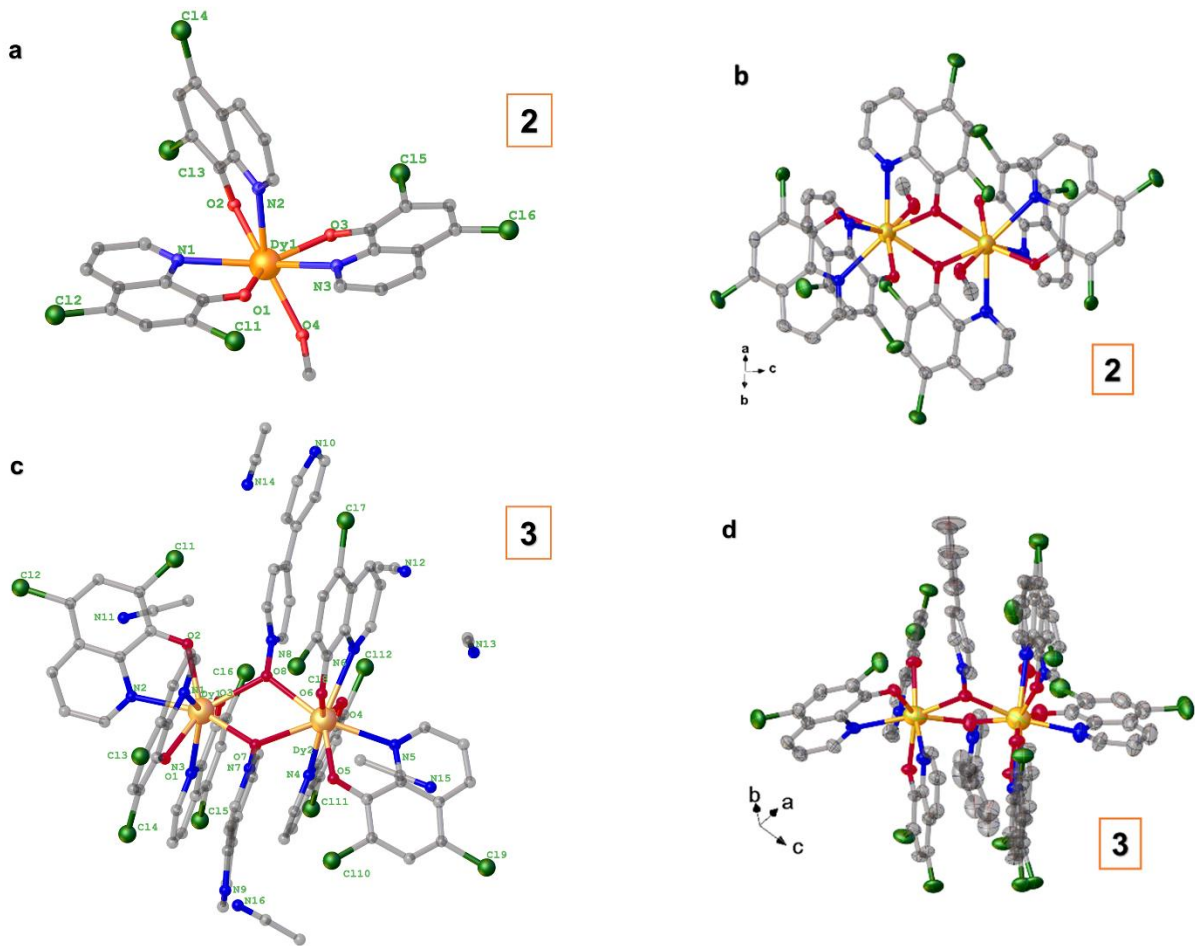


Figure S1. The asymmetric units of **2** (a) and **3** (c), and the complete molecule structures of **2** (b) and **3** (d) in ellipses & sticks mode.

Table S1. Selected bond lengths (\AA) and bond angles ($^\circ$) for **2**.

Dy(1)-O(1)	2.240(2)
Dy(1)-O(2)	2.314(2)
Dy(1)-O(3)	2.351(2)
Dy(1)-O(4)	2.373(2)
Dy(1)-O(3) [#]	2.422(2)
Dy(1)-N(1)	2.623(3)
Dy(1)-N(2)	2.547(3)
Dy(1)-N(3)	2.571(3)
O(3) ¹ -Dy(1)-O(3)	71.69(8)
O(3)-Dy(1)-O(3)	65.85(8)
Dy(1)- O(3)- Dy(1) [#]	108.30(8)
Dy(1)- O(3) [#] - Dy(1)	108.30 (8)
O(1)-Dy(1)-O(2)	131.28(8)
O(1)-Dy(1)-O(3)	139.63(8)
O(1)-Dy(1)-O(4)	80.54(8)
N(1)-Dy(1)-N(3)	135.08(9)
O(2)-Dy(1)-N(1)	70.96(8)
O(3)-Dy(1)-O(4)	84.42(18)
O(2)-Dy(1)-O(3)	130.59(8)

Symmetry code [#] 1-X, 1-Y, -Z

Table S2. Selected bond lengths (\AA) and bond angles ($^\circ$) for **3**.

Dy(1)-O(1)	2.244(5)	Dy(2)-O(4)	2.461(3)
Dy(1)-O(2)	2.246(4)	Dy(2)-O(5)	2.440(4)
Dy(1)-O(3)	2.299(4)	Dy(2)-O(6)	2.265(4)
Dy(1)-O(4)	2.433(4)	Dy(2)-O(7)	2.278(3)
Dy(1)-O(5)	2.460(4)	Dy(2)-O(8)	2.268(3)
Dy(1)-N(1)	2.600(7)	Dy(2)-N(4)	2.526(4)
Dy(1)-N(2)	2.497(5)	Dy(2)-N(5)	2.580(4)
Dy(1)-N(3)	2.615(6)	Dy(2)-N(6)	2.527(5)
O(1)-Dy(1)-O(4)	108.30(15)	O(7)-Dy(2)-O(4)	75.06(12)
Dy(1)-O(7)-Dy(5)	73.31(17)	O(7)-Dy(2)-O(5)	137.35(12)
O(1)-Dy(1)-O(2)	86.60(18)	O(7)-Dy(2)-N(5)	133.18(13)
O(1)-Dy(1)-O(3)	136.56(17)	O(4)-Dy(1)-N(6)	140.33(13)
O(1)-Dy(1)-N(1)	66.3(2)	O(4)-Dy(1)-N(1)	90.38(17)
O(1)-Dy(1)-N(2)	85.00(19)	O(4)-Dy(1)-N(5)	62.79(12)
O(3)-Dy(1)-O(4)	79.46(14)	O(4)-Dy(1)-N(2)	159.33(15)
O(2)-Dy(1)-O(3)	123.90(17)	O(4)-Dy(1)-O(5)	62.79(12)
O(2)-Dy(1)-N(1)	140.46(19)	O(6)-Dy(1)-O(7)	84.3(2)
O(2)-Dy(1)-N(3)	68.54(16)	N(1)-Dy(1)-N(3)	135.5(2)
O(2)-Dy(1)-N(3)	73.26(19)	N(2)-Dy(1)-N(1)	80.4(2)
O(5)-Dy(1)-N(1)	120.35(18)	N(2)-Dy(1)-N(3)	95.4(2)

Table S3. Continuous Shape Measure (CSM) analysis for eight-coordinated Dy³⁺ ions in **2** and **3**.

Eight-coordinated coordination sphere label	Shape	CSM parameters			Determined coordination geometry
		2	3_Dy1	3_Dy2	
OP-8	Octagon	28.723	33.429	21.358	
HPY-8	Heptagonal pyramid	22.313	31.551	23.417	
HBPY-8	Hexagonal bipyramid	15.373	11.728	8.577	
CU-8	Cube	13.586	15.869	12.328	
SAPR-8	Square antiprism	3.574	3.046	3.141	
TDD-8	Triangular dodecahedron (D _{2d})	2.677	2.651	1.494	TDD-8
JGBF-8	Johnson - Gyrobifastigium (J26)	12.442	10.847	27.000	
JETBPY-8	Johnson - Elongated triangular bipyramid (J14)	25.169	12.440	27.357	
JBTP-8	Johnson - Biaugmented trigonal prism (J50)	3.034	4.364	2.737	
BTPR-8	Biaugmented trigonal prism (C _{2v})	1.951	3.364	2.811	BTPR-8
JSD-8	Snub disphenoid (J84)	5.110	5.501	3.932	
TT-8	Triakis tetrahedron	14.395	8.673	13.049	
ETBPY-8	Elongated trigonal bipyramid (see 8)	20.261	23.002	22.719	

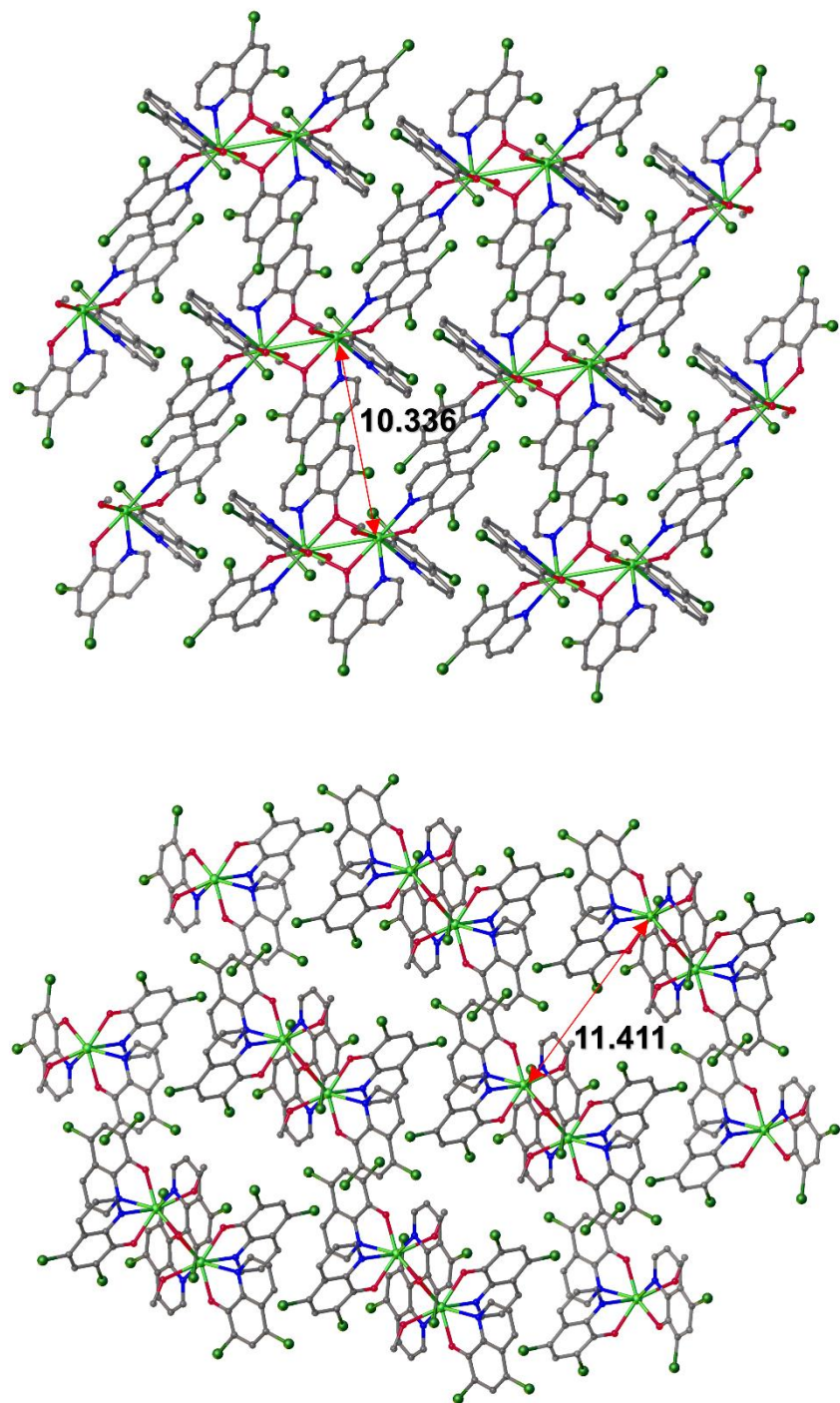


Figure S2. A portion of one-dimensional coordination chain structure of **2** along two main crystallographic axes: the *a* axis (*a*) and the *b* axis (*b*).

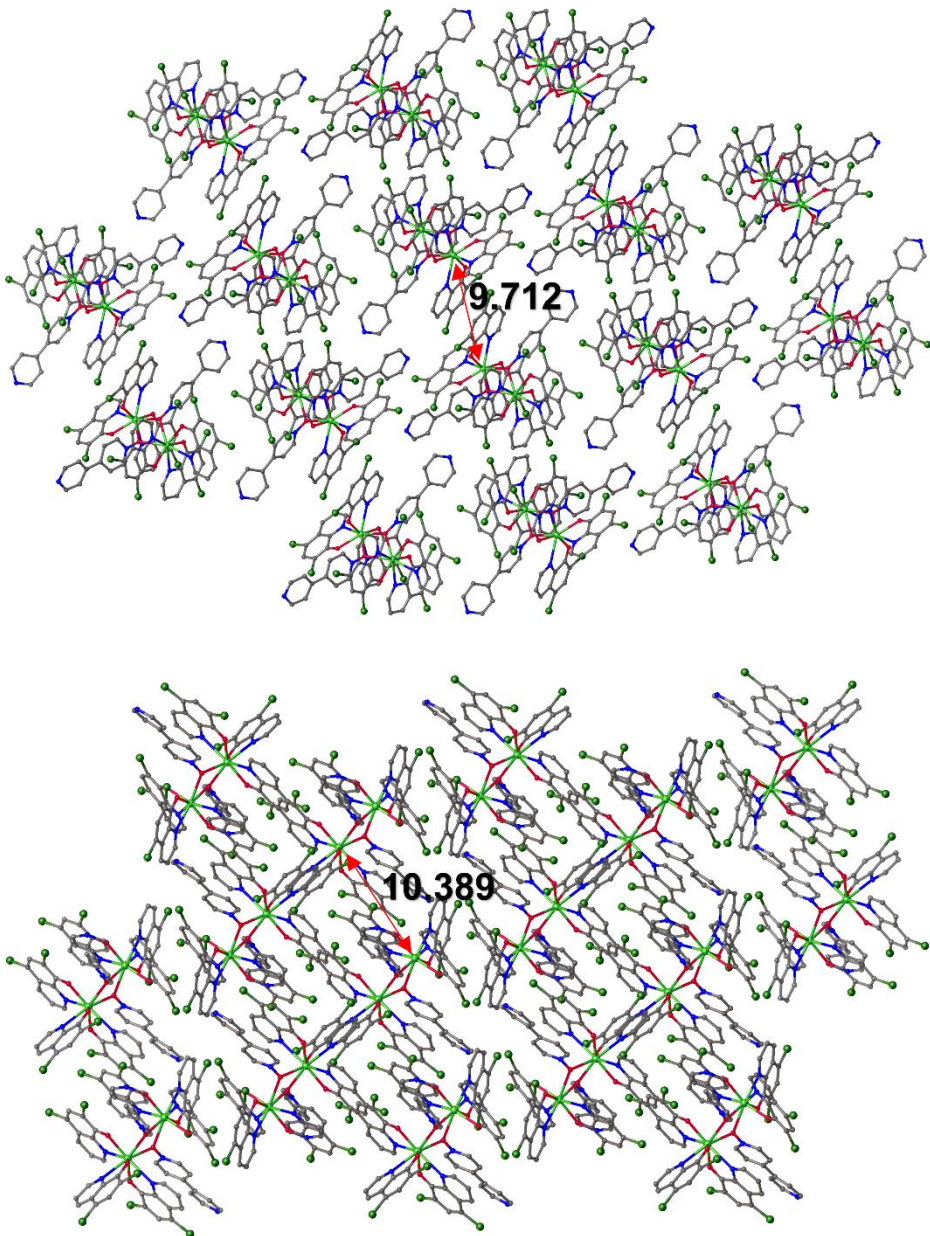


Figure S3. A portion of one-dimensional coordination chain structure of **3** along two main crystallographic axes: the *b* axis (a) and the *c* axis (b).

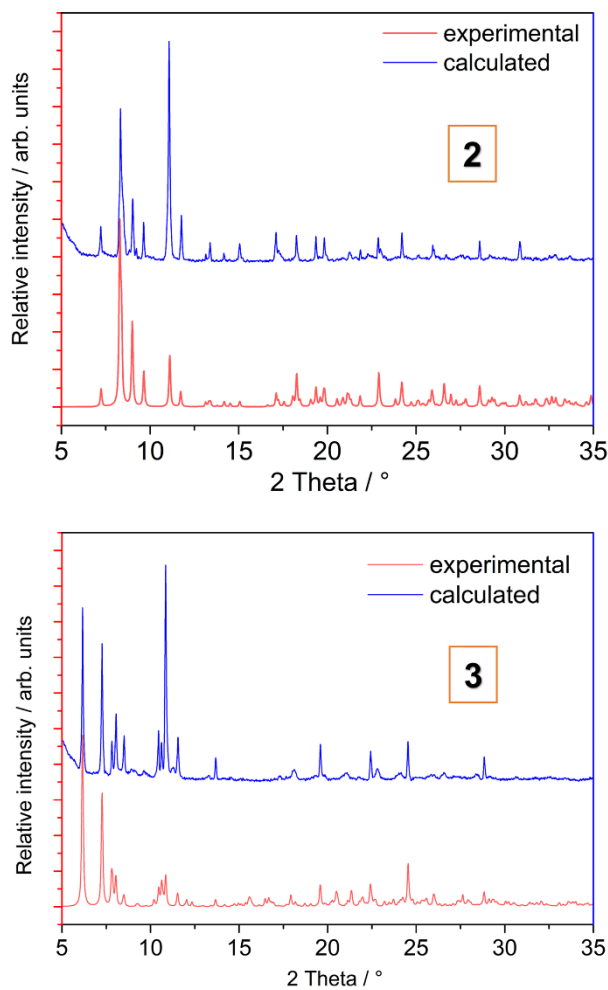


Figure S4. Comparison of the experimental PXRD patterns of **2** and **3** with the simulated patterns from single crystal structure. The calculated patterns were generated from Mercury using the CIF of the crystal structure.

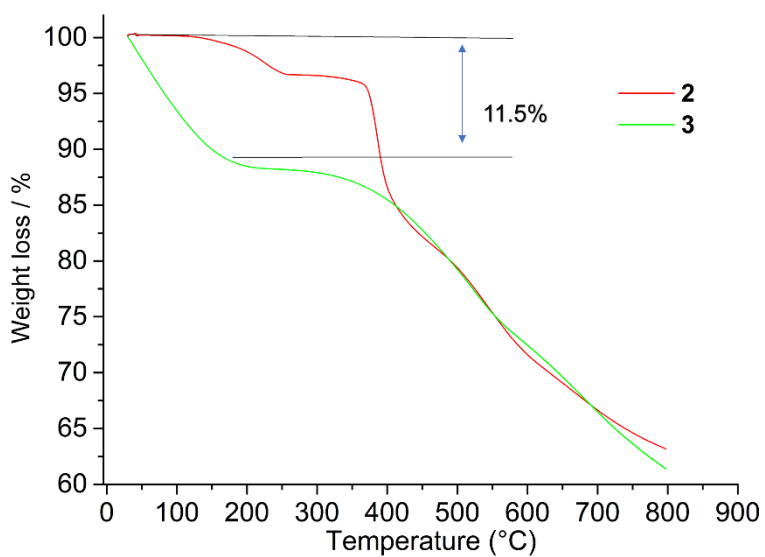


Figure S5. TGA curves of **2** and **3** measured under the Argon atmosphere upon the continuous heating with the $10\text{ }^{\circ}\text{C}\cdot\text{min}^{-1}$ rate.

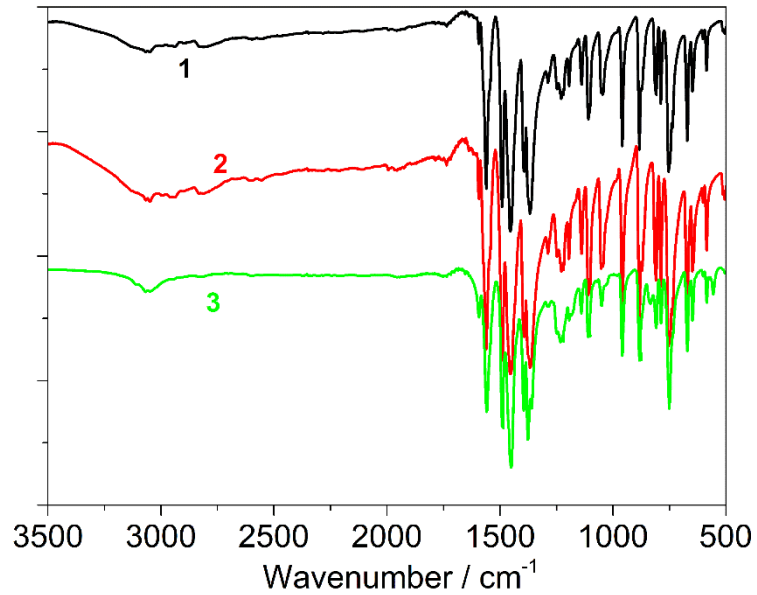


Figure S6. IR spectra of complexes **1**, **2** and **3**.

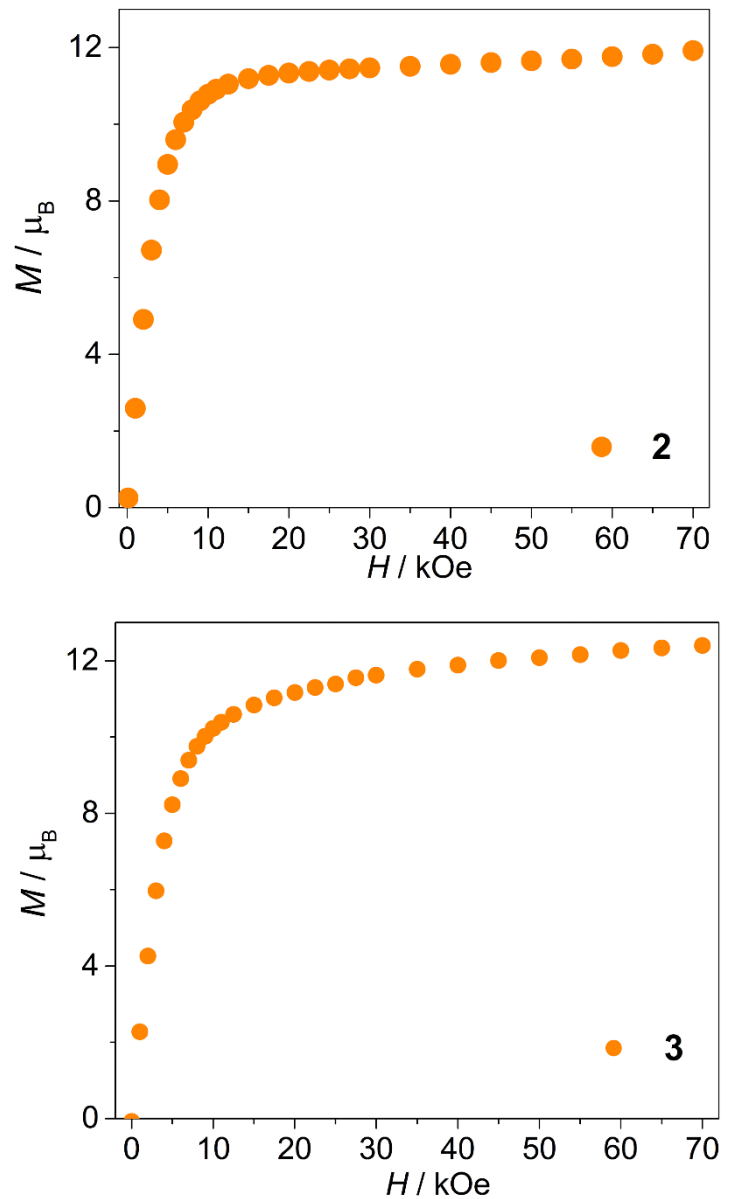


Figure S7. Variable-field magnetization at 2 K for **2** (up) and **3** (down).

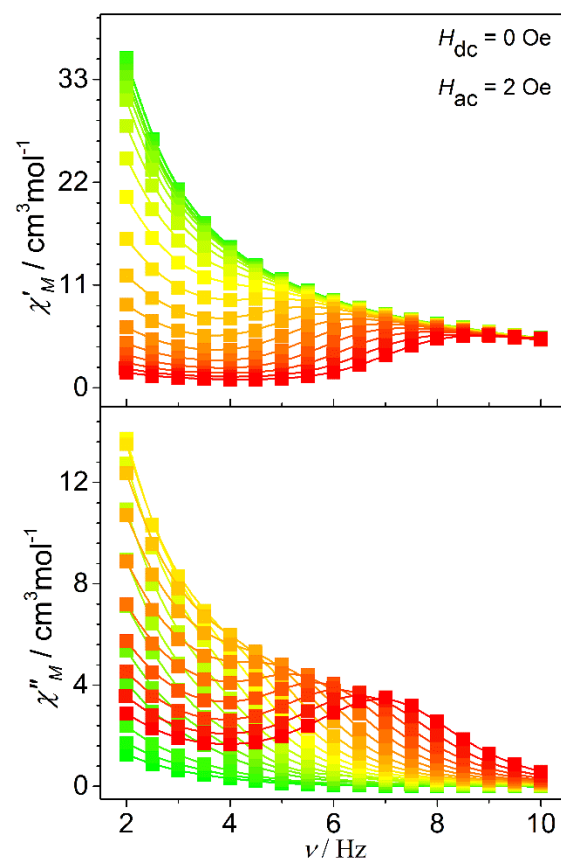


Figure S8. Temperature dependence of the in-phase (χ') and out-of-phase (χ'') part of the ac susceptibilities measured under zero dc field for **2**.

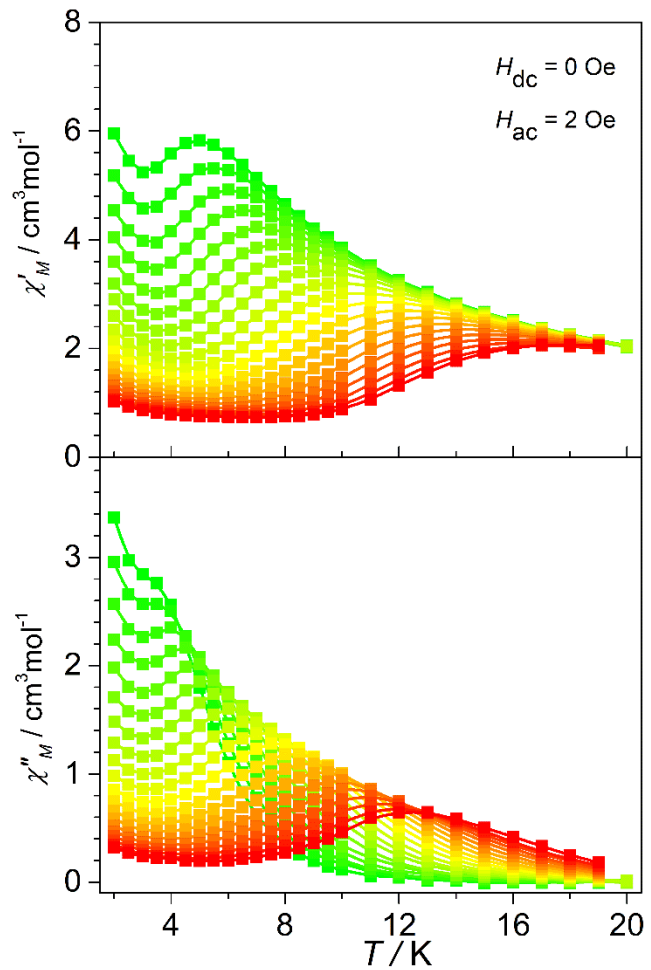


Figure S9. Temperature dependence of the in-phase (χ') and out-of-phase (χ'') part of the ac susceptibilities measured under zero dc field for **3**.

Table S4. Relaxation fitting parameters from the least-square fitting of the Cole-Cole plots of compound **2** under zero dc field according to the generalized Debye model.

T / K	$\chi_s / \text{cm}^3\text{mol}^{-1}\text{K}$	$\chi_T / \text{cm}^3\text{mol}^{-1}\text{K}$	τ / s	α
2	0.99552	35.7359	0.00349	0.15255
2.5	0.75456	26.9323	0.00325	0.15116
3	0.61482	21.4612	0.003	0.14947
3.5	0.54421	17.7841	0.00264	0.14176
4	0.46697	15.1422	0.00214	0.13107
4.5	0.38649	13.1158	0.00157	0.11519
5	0.28305	11.5667	0.00106	0.10339
5.5	0.14171	10.3488	6.8899E-4	0.09915
6	2.64889E-15	9.35583	4.40907E-4	0.0995
6.5	4.2425E-15	8.53939	2.8723E-4	0.09565
7	5.98864E-15	7.8498	1.86376E-4	0.09598
7.5	1.10377E-14	7.27112	1.20701E-4	0.10157

Table S5. Relaxation fitting parameters from the least-square fitting of the Cole-Cole plots of compound **3** under zero dc filed according to the generalized Debye model.

T / K	χ_s / cm ³ mol ⁻¹ K	χ_T / cm ³ mol ⁻¹ K	τ / s	α
4	0.61363	20.0792	1.42768	0.5271
4.5	0.69526	12.0725	0.25575	0.44148
5	0.70235	9.56305	0.11473	0.39137
5.5	0.68936	8.17385	0.06449	0.35693
6	0.66831	7.23857	0.04037	0.33388
6.5	0.64546	6.56804	0.02677	0.32036
7	0.62008	6.03673	0.01852	0.31381
7.5	0.60462	5.58438	0.01308	0.30312
8	0.58302	5.20952	0.00942	0.30104
8.5	0.57087	4.89198	0.00691	0.29901
9	0.55219	4.61368	0.00506	0.30003
9.5	0.5412	4.35761	0.00373	0.30365
10	0.52897	4.14935	0.00277	0.31248
11	0.51939	3.94914	0.00201	0.32102
12	0.52198	3.61075	0.00109	0.34454
13	0.58327	3.31572	6.13652E-4	0.36259
14	0.64933	3.07554	3.51084E-4	0.37682
15	0.70607	2.8598	1.94661E-4	0.38856

Table S6. RASSI-SO computed low-lying 21 spin-free sextet states and the spin-orbit coupled (Kramer doublets) for Dy center in monomer complex **1**. All the values are reported here in cm^{-1} . The values in red colour are for the spin-free sextet states while the values in the blue colour are for the spin-orbit coupled states.

Dy		
SPIN-FREE STATES	SPIN-ORBIT COUPLED STATES	
0.0	0.0	9666.8
17.4	57.6	9715.8
86.9	94.5	9778.2
116.6	137.9	9853.8
130.6	188.2	11007.5
253.7	244.1	11159.9
275.8	331.9	11248.6
355.3	420.9	11752.1
380.0	3029.3	11775.8
480.7	3087.9	11798.3
496.1	3122.9	11817.5
7531.8	3173.9	11837.2
7560.5	3224.9	13539.2
7628.9	3264.5	13558.8
7688.1	3302.5	13610.0
7722.8	5640.9	13633.6
7739.3	5695.3	14951.4
7752.8	5742.6	14971.2
34649.0	5789.8	15011.2
34863.0	5814.4	15972.3
35047.5	5875.9	15979.9
	7851.6	16573.2
	7893.0	38678.3
	7953.7	38738.7
	7983.9	38791.4
	8058.8	38886.7
	9523.4	40069.4
	9557.0	40181.4
	9586.6	40306.8
	9613.2	41165.5
	9625.9	41210.6
	9652.2	

Table S7. RASSI-SO computed low-lying 21 spin-free sextet states and the spin-orbit coupled (Kramer doublets) for Dy@1 center in dimer complex **2**. All the values are reported here in cm⁻¹. The values in red colour are for the spin-free sextet states while the values in the blue colour are for the spin-orbit coupled states.

Dy@1		
SPIN-FREE STATES	SPIN-ORBIT COUPLED STATES	
0.0	0.0	9837.8
18.8	99.6	9877.6
129.5	163.7	9927.0
161.7	257.5	10149.8
229.1	354.4	11065.2
285.2	434.9	11266.5
442.4	593.5	11571.8
567.2	777.8	11890.8
591.6	3044.1	11932.1
823.3	3149.4	11970.5
830.4	3247.9	11997.2
7629.5	3293.9	12016.2
7709.9	3372.2	13705.5
7762.0	3493.4	13729.1
7820.7	3669.3	13764.6
7877.9	5679.6	13802.2
7912.1	5789.1	15122.1
7928.8	5848.8	15136.1
34597.2	5928.5	15173.5
34894.4	6025.1	16125.0
35506.5	6201.1	16158.7
	7905.7	16745.9
	8005.6	38681.9
	8062.8	38822.1
	8174.2	38935.5
	8354.1	39122.4
	9628.4	40111.5
	9683.3	40301.9
	9724.4	40702.0
	9742.3	41372.2
	9781.1	41462.7
	9815.7	

Table S8. RASSI-SO computed low-lying 21 spin-free sextet states and the spin-orbit coupled (Kramer doublets) for Dy@2 center in dimer complex **2**. All the values are reported here in cm⁻¹. The values in red colour are for the spin-free sextet states while the values in the blue colour are for the spin-orbit coupled states.

Dy@2		
SPIN-FREE STATES	SPIN-ORBIT COUPLED STATES	
0.0	0.0	9837.7
18.7	99.5	9877.5
129.3	163.5	9926.9
161.5	257.4	10149.7
228.9	354.3	11065.2
285.1	434.9	11266.4
442.3	593.5	11571.7
567.1	777.7	11890.7
591.5	3044.0	11932.0
823.2	3149.3	11970.4
830.3	3247.8	11997.1
7629.4	3293.7	12016.0
7709.8	3372.1	13705.4
7761.9	3493.3	13729.0
7820.6	3669.2	13764.5
7877.8	5679.5	13802.1
7911.9	5789.0	15122.0
7928.7	5848.7	15136.0
34597.2	5928.4	15173.4
34894.1	6025.0	16124.9
35506.4	6201.0	16158.6
	7905.7	16745.8
	8005.5	38681.8
	8062.7	38822.0
	8174.1	38935.5
	8354.1	39122.2
	9628.3	40111.3
	9683.2	40301.7
	9724.3	40701.9
	9742.2	41372.1
	9781.0	41462.6
	9815.6	

Table S9. RASSI-SO computed low-lying 21 spin-free sextet states and the spin-orbit coupled (Kramer doublets) for Dy@1 center in dimer complex **3**. All the values are reported here in cm⁻¹. The values in red colour are for the spin-free sextet states while the values in the blue colour are for the spin-orbit coupled states.

Dy@1		
SPIN-FREE STATES	SPIN-ORBIT COUPLED STATES	
0.0	0.0	9777.5
21.3	51.7	9831.6
75.0	179.3	9892.9
96.2	251.2	9998.4
228.8	312.9	11045.5
325.9	364.6	11251.0
354.7	439.7	11402.9
469.3	611.4	11835.1
494.5	3029.0	11870.1
653.2	3145.4	11905.3
669.6	3203.7	11934.4
7564.6	3272.4	11948.8
7666.7	3339.8	13622.2
7680.9	3391.3	13672.6
7753.9	3474.9	13716.7
7803.0	5645.9	13733.5
7845.7	5780.7	15051.9
7860.7	5821.3	15072.6
34564.1	5886.9	15111.2
35023.1	5961.0	16070.0
35204.2	6017.6	16083.6
	7864.7	16676.7
	7989.8	38707.0
	8036.7	38770.5
	8118.7	38860.7
	8188.4	39065.1
	9593.3	40113.5
	9635.8	40309.3
	9663.9	40472.1
	9697.4	41270.1
	9707.5	41345.1
	9743.2	

Table S10. RASSI-SO computed low-lying 21 spin-free sextet states and the spin-orbit coupled (Kramer doublets) for Dy@2 center in dimer complex **3**. All the values are reported here in cm⁻¹. The values in red colour are for the spin-free sextet states while the values in the blue colour are for the spin-orbit coupled states.

Dy@2		
SPIN-FREE STATES	SPIN-ORBIT COUPLED STATES	
0.0	0.0	9782.7
5.5	94.9	9844.6
120.3	193.3	9870.3
143.3	268.9	10037.2
249.1	332.5	11069.0
357.0	421.0	11260.1
394.5	469.0	11441.1
491.6	623.7	11861.0
503.2	3051.0	11893.4
652.2	3165.1	11911.4
667.6	3230.5	11943.7
7610.2	3299.2	11967.3
7631.2	3339.8	13656.6
7719.5	3402.7	13674.6
7790.5	3526.0	13729.2
7817.2	5682.5	13755.6
7845.1	5802.1	15067.3
7861.2	5840.7	15092.2
34608.5	5892.7	15129.7
34921.6	5950.2	16085.6
35286.9	6078.5	16103.7
	7906.3	16693.8
	8010.2	38705.7
	8042.6	38805.5
	8106.3	38889.9
	8245.0	39053.2
	9612.2	40117.2
	9661.4	40280.7
	9698.3	40527.4
	9721.8	41288.7
	9743.9	41361.8
	9769.1	

Table S11. SINGLE_ANISO computed g-tensors, the angle of deviation from ground state g_{zz} orientation, and relative energies of eight low lying Kramers' doublets for Dy center in monomer complex **1**.

Dy				
KDs Energy (cm ⁻¹)	g_{xx}	g_{yy}	g_{zz}	θ (° angle)
0.0	0.2480	0.6467	18.5807	0.0
57.6	1.7523	2.8039	14.1775	17.0
94.5	2.9003	3.8871	12.4226	42.9
137.9	1.7043	4.3565	9.3575	82.3
188.2	1.2167	1.5813	14.1226	94.6
244.1	0.1385	0.2093	18.4399	54.3
331.9	0.0239	0.1171	19.2682	100.0
420.9	0.0329	0.0835	19.6826	68.3

Table S12. SINGLE_ANISO computed g-tensors, the angle of deviation from ground state g_{zz} orientation, and relative energies of eight low lying Kramers' doublets for Dy@1 and Dy@2 centers in dimer complex **2**.

Dy@1				Dy@2				
KDs Energy (cm ⁻¹)	g_{xx}	g_{yy}	g_{zz}	θ (° angle)	KDs Energy (cm ⁻¹)	g_{xx}	g_{yy}	g_{zz}
0.0	0.0254	0.0484	19.6737	0.0	0.0	0.0254	0.0484	19.6699
99.6	0.1771	0.3674	16.5527	8.4	99.5	0.1789	0.3709	16.5485
163.7	0.7027	1.2453	15.5833	127.6	163.5	0.7007	1.2471	15.5760
257.5	1.1685	3.1266	10.2062	23.7	257.4	1.1727	3.1300	10.2020
354.4	7.0753	5.6282	3.7901	83.2	354.3	7.0800	5.6257	3.7910
434.9	1.8167	3.7845	13.0162	85.2	434.9	1.8134	3.7784	13.0227
593.5	0.1127	0.1756	17.3443	92.0	593.5	0.1126	0.1757	17.3436
777.8	0.0080	0.0124	19.7265	83.0	777.7	0.0080	0.0124	19.7236

NOTE: The angle of deviation from the ground state g_{zz} orientation for both the Dy centers was of the same magnitude, as the complex **2** is centrosymmetric.

Table S13. SINGLE_ANISO computed g-tensors, the angle of deviation from ground state g_{zz} orientation, and relative energies of eight low lying Kramers' doublets for Dy@1 and Dy@2 centers in dimer complex **3**.

Dy@1					
KDs	Energy (cm ⁻¹)	g_{xx}	g_{yy}	g_{zz}	θ (° angle)
	0.0	0.0913	0.2271	19.1102	0.0
	51.7	0.0216	0.2364	17.0380	8.5
	179.3	1.1409	1.2443	15.0004	19.7
	251.2	5.0226	5.9569	9.1270	36.3
	312.9	1.8906	3.7837	11.6121	97.0
	364.6	0.1930	0.4813	17.0501	90.9
	439.7	0.0857	0.1999	19.5269	79.3
	611.4	0.0177	0.0323	19.8246	106.3
Dy@2					
KDs	Energy (cm ⁻¹)	g_{xx}	g_{yy}	g_{zz}	θ (° angle)
	0.0	0.0083	0.0141	19.7057	0.0
	94.9	0.0310	0.0435	17.9333	35.0
	193.3	0.3003	0.3681	13.7816	28.2
	268.9	3.1558	4.7047	9.2111	38.1
	332.5	3.3438	5.0141	10.1447	90.5
	421.0	0.1057	0.5768	15.5528	108.6
	469.0	0.1863	0.5527	17.5004	85.2
	623.7	0.0063	0.0116	19.7976	114.4

Table S14. SINGLE_ANISO computed crystal field parameters for Dy center in monomer complex **1**. The major dominating values are kept in bold.

k	q	B_k^q
		Dy
2	-2	-6.70E-01
	-1	-2.10E+00
	0	-1.30E+00
	1	-3.40E-01
	2	1.50E+00
4	-4	5.20E-03
	-3	-4.70E-02
	-2	-1.00E-02
	-1	1.90E-02
	0	-1.10E-03
	1	-1.00E-02
	2	7.50E-03
	3	-4.20E-02
	4	-2.70E-02
6	-6	8.50E-05
	-5	3.30E-04
	-4	-5.10E-05
	-3	1.90E-04
	-2	1.70E-04
	-1	-8.50E-05
	0	-5.00E-07
	1	1.00E-04
	2	6.30E-05
	3	-1.00E-04
	4	-1.00E-04
	5	-2.50E-04
	6	-4.10E-05

Table S15. SINGLE_ANISO computed crystal field parameters for Dy@1 and Dy@2 centers in both dimer complexes **2** and **3** respectively. The major dominating values are kept in bold.

k	q	B_k^q	B_k^q	B_k^q	B_k^q
		Complex 2		Complex 3	
		Dy@1	Dy@2	Dy@1	Dy@2
2	-2	2.10E+00	2.10E+00	7.60E-01	-6.90E-01
	-1	-1.20E+00	-1.20E+00	1.20E+00	2.80E+00
	0	-3.00E+00	-3.00E+00	-2.60E+00	-2.20E+00
	1	-6.50E-01	-6.60E-01	2.90E+00	-2.40E+00
	2	4.10E+00	4.10E+00	9.20E-01	2.80E+00
4	-4	7.50E-03	7.50E-03	3.30E-03	-9.60E-03
	-3	4.00E-02	4.00E-02	4.30E-02	-4.60E-04
	-2	-6.60E-03	-6.60E-03	-3.00E-03	8.10E-03
	-1	1.20E-02	1.20E-02	-1.10E-02	-1.70E-02
	0	-1.00E-03	-1.00E-03	5.10E-04	-3.30E-03
	1	4.30E-03	4.30E-03	-1.80E-02	-7.10E-04
	2	3.10E-03	3.10E-03	1.30E-02	1.50E-02
	3	-6.30E-02	-6.30E-02	-5.10E-02	-7.20E-02
	4	1.00E-02	1.00E-02	-2.70E-02	2.00E-03
6	-6	-2.40E-05	-2.40E-05	-1.20E-04	-3.10E-05
	-5	1.30E-05	2.00E-05	3.10E-04	-2.80E-04
	-4	1.60E-05	1.60E-05	-5.80E-06	-8.60E-05
	-3	-4.20E-04	-4.20E-04	-3.50E-04	-1.30E-04
	-2	-9.40E-05	-9.40E-05	-2.10E-05	-1.10E-04
	-1	-1.10E-04	-1.10E-04	-2.60E-05	-1.00E-04
	0	1.50E-05	1.50E-05	2.40E-05	1.10E-06
	1	-3.60E-05	-3.60E-05	5.90E-05	1.90E-04
	2	3.10E-05	3.10E-05	1.40E-04	-1.00E-04
	3	1.60E-04	1.60E-04	3.60E-04	1.80E-05
	4	1.00E-04	1.00E-04	-1.30E-06	1.00E-04
	5	-1.10E-03	-1.10E-03	-4.70E-04	-6.10E-04
	6	-1.90E-05	-1.90E-05	1.40E-04	-5.80E-05

Table S16. SINGLE_ANISO computed wave function decomposition analysis for Dy center in monomer complex **1**. The major dominating values are kept in bold.

$\pm m_J$	<i>wave function decomposition analysis Dy</i>
KD1	82.0% $ \pm 15/2\rangle$ + 10.7% $ \pm 11/2\rangle$ + 4.5% $ \pm 7/2\rangle$
KD2	58.3% $ \pm 13/2\rangle$ + 20.6% $ \pm 9/2\rangle$ + 10.2% $ \pm 5/2\rangle$
KD3	25.4% $ \pm 11/2\rangle$ + 22.3% $ \pm 7/2\rangle$ + 14.1% $ \pm 13/2\rangle$ + 8.6% $ \pm 3/2\rangle$ + 8.5% $ \pm 15/2\rangle$ + 8.3% $ \pm 9/2\rangle$ + 7.4% $ \pm 5/2\rangle$ + 5.1% $ \pm 1/2\rangle$
KD4	20.5% $ \pm 11/2\rangle$ + 17.0% $ \pm 3/2\rangle$ + 15.8% $ \pm 5/2\rangle$ + 14.5% $ \pm 9/2\rangle$ + 11.9% $ \pm 1/2\rangle$ + 9.3% $ \pm 7/2\rangle$ + 7.8% $ \pm 13/2\rangle$
KD5	23.0% $ \pm 1/2\rangle$ + 21.8% $ \pm 3/2\rangle$ + 20.4% $ \pm 5/2\rangle$ + 15.1% $ \pm 7/2\rangle$ + 6.3% $ \pm 9/2\rangle$ + 6.3% $ \pm 11/2\rangle$ + 5.2% $ \pm 13/2\rangle$
KD6	28.2% $ \pm 9/2\rangle$ + 24.9% $ \pm 11/2\rangle$ + 12.8% $ \pm 7/2\rangle$ + 11.5% $ \pm 13/2\rangle$ + 10.4% $ \pm 1/2\rangle$ + 6.0% $ \pm 3/2\rangle$
KD7	34.2% $ \pm 1/2\rangle$ + 23.9% $ \pm 3/2\rangle$ + 17.4% $ \pm 5/2\rangle$ + 14.0% $ \pm 7/2\rangle$ + 7.3% $ \pm 9/2\rangle$
KD8	24.4% $ \pm 5/2\rangle$ + 20.5% $ \pm 7/2\rangle$ + 20.0% $ \pm 3/2\rangle$ + 13.4% $ \pm 9/2\rangle$ + 11.9% $ \pm 1/2\rangle$ + 7.0% $ \pm 11/2\rangle$

Table S17. SINGLE_ANISO computed wave function decomposition analysis for Dy@1 and Dy@2 centers in dimeric complex **2**. The major dominating values are kept in bold.

$\pm m_J$	wave function decomposition analysis Dy@1
KD1	94.9% $ \pm 15/2\rangle$ + 4.6% $ \pm 11/2\rangle$
KD2	85.7% $ \pm 13/2\rangle$ + 10.5% $ \pm 9/2\rangle$
KD3	26.7% $ \pm 11/2\rangle$ + 21.0% $ \pm 7/2\rangle$ + 15.8% $ \pm 5/2\rangle$ + 12.9% $ \pm 3/2\rangle$ + 8.7% $ \pm 9/2\rangle$ + 7.7% $ \pm 1/2\rangle$
KD4	51.6% $ \pm 11/2\rangle$ + 18.2% $ \pm 1/2\rangle$ + 12.3% $ \pm 3/2\rangle$ + 7.7% $ \pm 5/2\rangle$ + 5.5% $ \pm 9/2\rangle$
KD5	43.9% $ \pm 9/2\rangle$ + 17.4% $ \pm 1/2\rangle$ + 13.6% $ \pm 3/2\rangle$ + 9.1% $ \pm 5/2\rangle$ + 7.6% $ \pm 7/2\rangle$
KD6	34.0% $ \pm 7/2\rangle$ + 15.9% $ \pm 5/2\rangle$ + 15.7% $ \pm 1/2\rangle$ + 13.6% $ \pm 9/2\rangle$ + 13.2% $ \pm 3/2\rangle$ + 6.6% $ \pm 11/2\rangle$
KD7	31.7% $ \pm 5/2\rangle$ + 24.5% $ \pm 7/2\rangle$ + 20.1% $ \pm 3/2\rangle$ + 12.1% $ \pm 9/2\rangle$ + 6.5% $ \pm 1/2\rangle$ + 4.0% $ \pm 11/2\rangle$
KD8	34.2% $ \pm 1/2\rangle$ + 27.8% $ \pm 3/2\rangle$ + 18.8% $ \pm 5/2\rangle$ + 11.0% $ \pm 7/2\rangle$ + 5.5% $ \pm 9/2\rangle$
$\pm m_J$	wave function decomposition analysis Dy@2
KD1	94.9% $ \pm 15/2\rangle$ + 4.6% $ \pm 11/2\rangle$
KD2	85.7% $ \pm 13/2\rangle$ + 10.5% $ \pm 9/2\rangle$
KD3	26.7% $ \pm 11/2\rangle$ + 21.0% $ \pm 7/2\rangle$ + 15.8% $ \pm 5/2\rangle$ + 12.9% $ \pm 3/2\rangle$ + 8.7% $ \pm 9/2\rangle$ + 7.7% $ \pm 1/2\rangle$
KD4	51.7% $ \pm 11/2\rangle$ + 18.2% $ \pm 1/2\rangle$ + 12.3% $ \pm 3/2\rangle$ + 7.7% $ \pm 5/2\rangle$ + 5.5% $ \pm 9/2\rangle$
KD5	43.9% $ \pm 9/2\rangle$ + 17.4% $ \pm 1/2\rangle$ + 13.6% $ \pm 3/2\rangle$ + 9.1% $ \pm 5/2\rangle$ + 7.6% $ \pm 7/2\rangle$
KD6	33.9% $ \pm 7/2\rangle$ + 15.9% $ \pm 5/2\rangle$ + 15.7% $ \pm 1/2\rangle$ + 13.6% $ \pm 9/2\rangle$ + 13.2% $ \pm 3/2\rangle$ + 6.6% $ \pm 11/2\rangle$
KD7	31.7% $ \pm 5/2\rangle$ + 24.5% $ \pm 7/2\rangle$ + 20.1% $ \pm 3/2\rangle$ + 12.1% $ \pm 9/2\rangle$ + 6.5% $ \pm 1/2\rangle$ + 4.0% $ \pm 11/2\rangle$
KD8	34.2% $ \pm 1/2\rangle$ + 27.8% $ \pm 3/2\rangle$ + 18.8% $ \pm 5/2\rangle$ + 11.0% $ \pm 7/2\rangle$ + 5.5% $ \pm 9/2\rangle$

Table S18. SINGLE_ANISO computed wave function decomposition analysis for Dy@1 and Dy@2 centers in dimeric complex **3**. The major dominating values are kept in bold.

$\pm mJ$	wave function decomposition analysis Dy@1
KD1	85.2% $ \pm 15/2\rangle$ + 13.5% $ \pm 11/2\rangle$
KD2	91.6% $ \pm 13/2\rangle$ + 5.1% $ \pm 9/2\rangle$
KD3	65.3% $ \pm 11/2\rangle$ + 14.3% $ \pm 9/2\rangle$ + 12.0% $ \pm 15/2\rangle$ + 4.2% $ \pm 5/2\rangle$
KD4	37.4% $ \pm 9/2\rangle$ + 27.4% $ \pm 7/2\rangle$ + 13.2% $ \pm 3/2\rangle$ + 6.3% $ \pm 1/2\rangle$ + 6.1% $ \pm 11/2\rangle$ + 4.3% $ \pm 5/2\rangle$
KD5	24.2% $ \pm 5/2\rangle$ + 20.2% $ \pm 7/2\rangle$ + 19.3% $ \pm 9/2\rangle$ + 18.1% $ \pm 1/2\rangle$ + 8.0% $ \pm 11/2\rangle$ + 7.7% $ \pm 3/2\rangle$
KD6	24.3% $ \pm 1/2\rangle$ + 24.1% $ \pm 3/2\rangle$ + 20.6% $ \pm 5/2\rangle$ + 20.3% $ \pm 7/2\rangle$ + 9.3% $ \pm 9/2\rangle$
KD7	31.0% $ \pm 3/2\rangle$ + 28.6% $ \pm 1/2\rangle$ + 22.6% $ \pm 5/2\rangle$ + 10.8% $ \pm 7/2\rangle$ + 4.9% $ \pm 9/2\rangle$
KD8	23.8% $ \pm 5/2\rangle$ + 22.9% $ \pm 3/2\rangle$ + 21.8% $ \pm 1/2\rangle$ + 19.5% $ \pm 7/2\rangle$ + 9.3% $ \pm 9/2\rangle$
$\pm mJ$	wave function decomposition analysis Dy@2
KD1	95.5% $ \pm 15/2\rangle$ + 3.5% $ \pm 11/2\rangle$
KD2	48.9% $ \pm 13/2\rangle$ + 19.4% $ \pm 9/2\rangle$ + 18.4% $ \pm 11/2\rangle$ + 8.4% $ \pm 7/2\rangle$
KD3	38.6% $ \pm 13/2\rangle$ + 21.0% $ \pm 7/2\rangle$ + 10.8% $ \pm 11/2\rangle$ + 10.9% $ \pm 5/2\rangle$ + 8.8% $ \pm 3/2\rangle$
KD4	34.5% $ \pm 11/2\rangle$ + 23.1% $ \pm 1/2\rangle$ + 21.1% $ \pm 5/2\rangle$ + 10.2% $ \pm 3/2\rangle$ + 6.1% $ \pm 9/2\rangle$
KD5	30.2% $ \pm 3/2\rangle$ + 24.4% $ \pm 9/2\rangle$ + 13.0% $ \pm 1/2\rangle$ + 11.1% $ \pm 11/2\rangle$ + 9.2% $ \pm 7/2\rangle$ + 8.2% $ \pm 5/2\rangle$
KD6	30.9% $ \pm 7/2\rangle$ + 20.2% $ \pm 1/2\rangle$ + 18.1% $ \pm 5/2\rangle$ + 18.0% $ \pm 9/2\rangle$ + 6.1% $ \pm 11/2\rangle$ + 5.4% $ \pm 3/2\rangle$
KD7	30.2% $ \pm 3/2\rangle$ + 28.7% $ \pm 1/2\rangle$ + 20.4% $ \pm 5/2\rangle$ + 8.6% $ \pm 7/2\rangle$ + 5.8% $ \pm 9/2\rangle$ + 4.2% $ \pm 11/2\rangle$
KD8	20.8% $ \pm 7/2\rangle$ + 19.1% $ \pm 9/2\rangle$ + 18.6% $ \pm 5/2\rangle$ + 14.7% $ \pm 3/2\rangle$ + 11.7% $ \pm 1/2\rangle$ + 11.1% $ \pm 11/2\rangle$

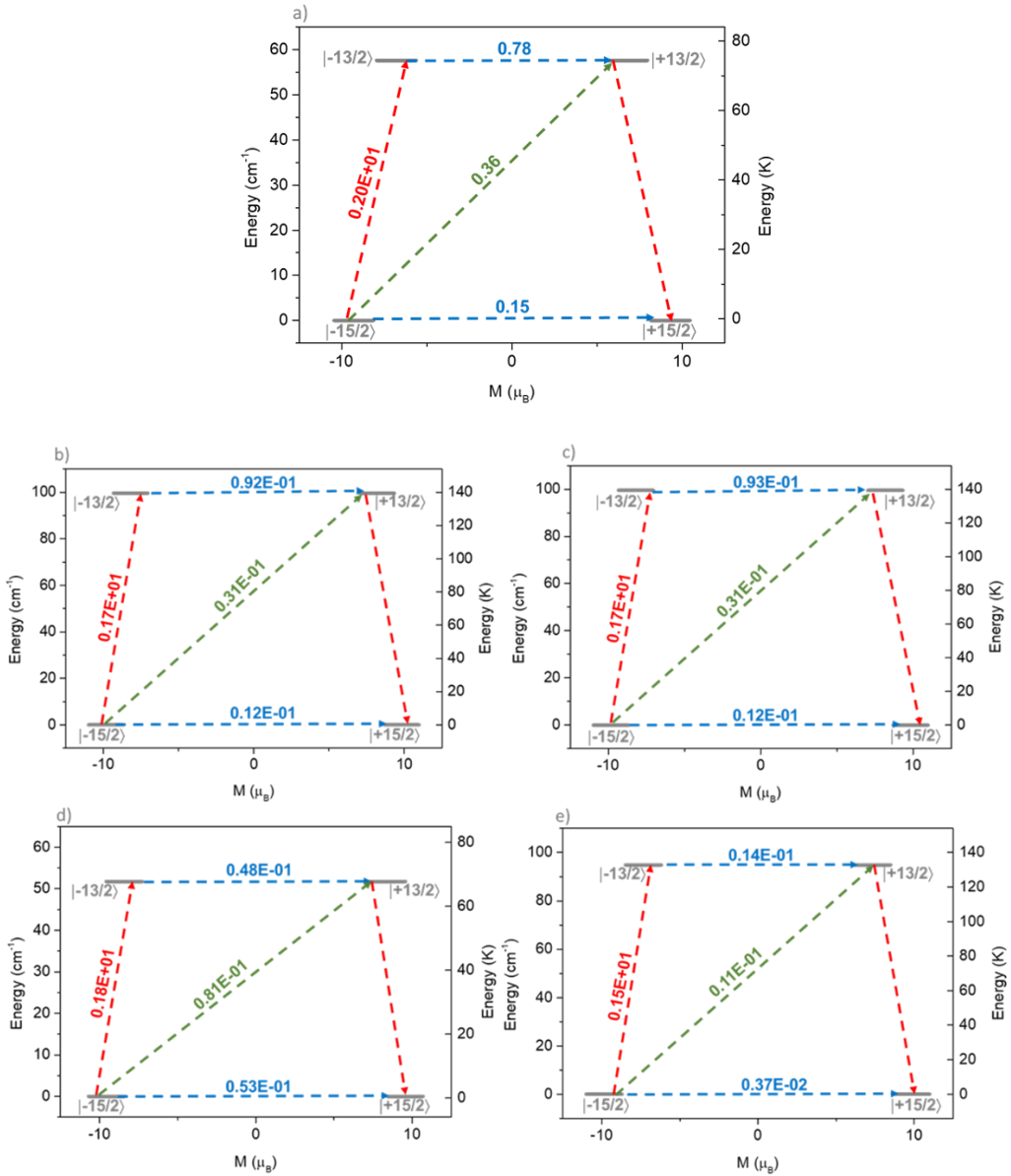


Figure S10. Ab initio computed magnetic relaxation pathway for the (a) Dy center in monomer complex **1**; (b) Dy@1 and (c) Dy@2 centers in dimer complex **2**; and (d) Dy@1 and Dy@2 centers in dimer complex **3** respectively. The grey horizontal bars indicate the KDs as magnetic moments' function. The blue, red, and green arrows represent the possible QTM/TA-QTM, Orbach, and Raman relaxation pathways.

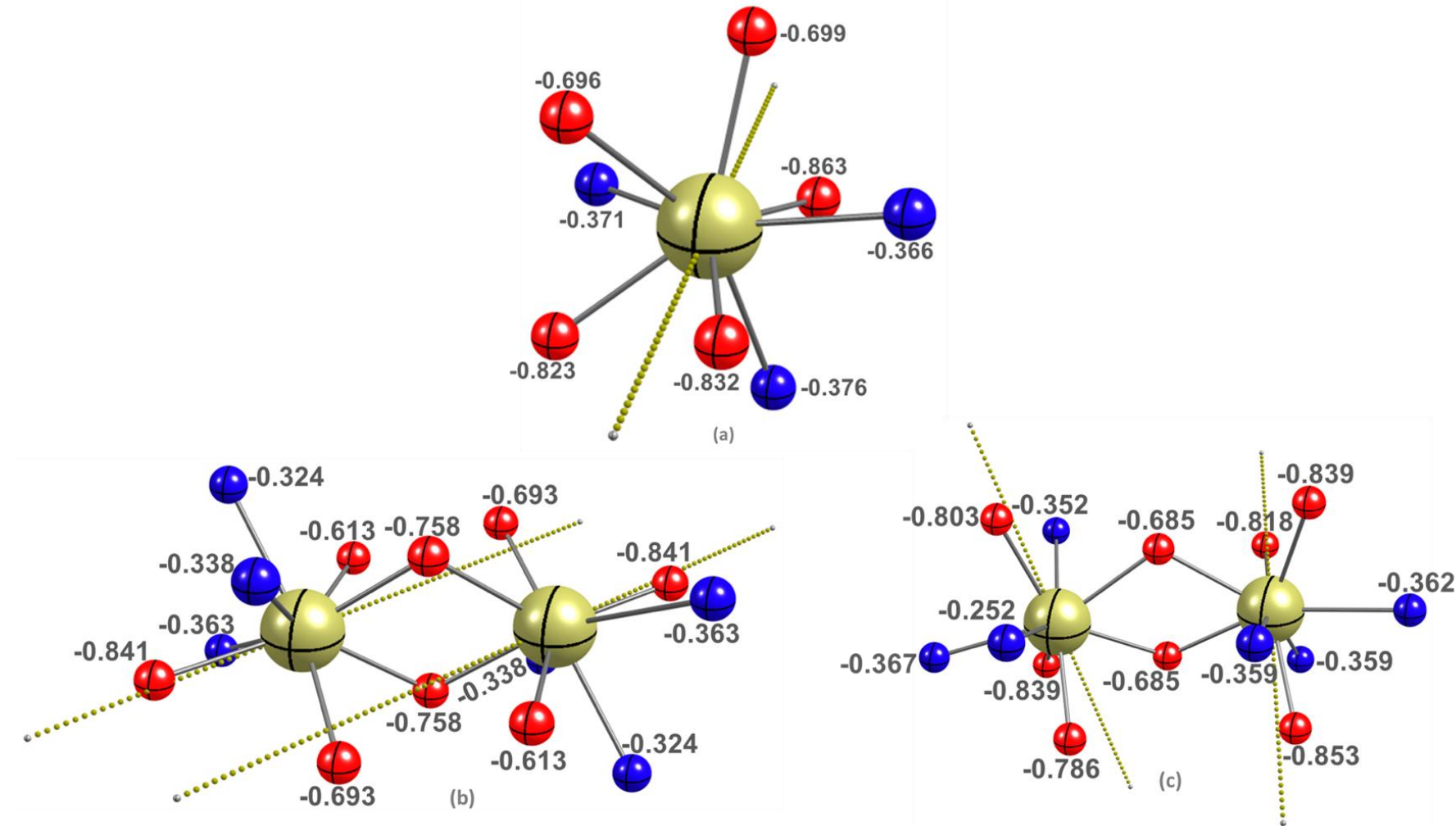


Figure S11. CASSCF computed LoProp charges on the first coordinating atoms of Dy centers in (a) monomeric complex **1**; (b) dimeric complex **2**, and (c) dimeric complex **3** respectively.

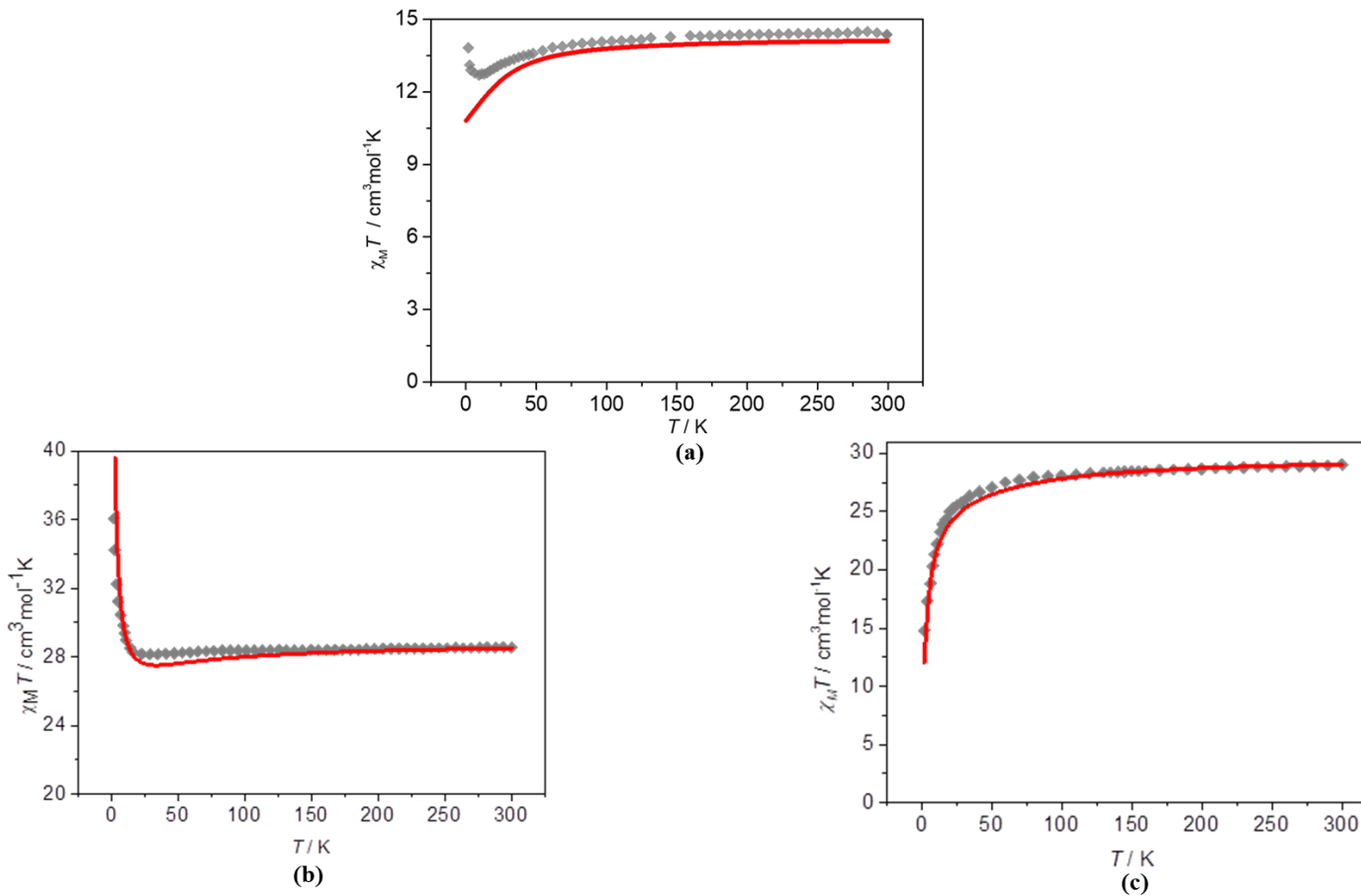
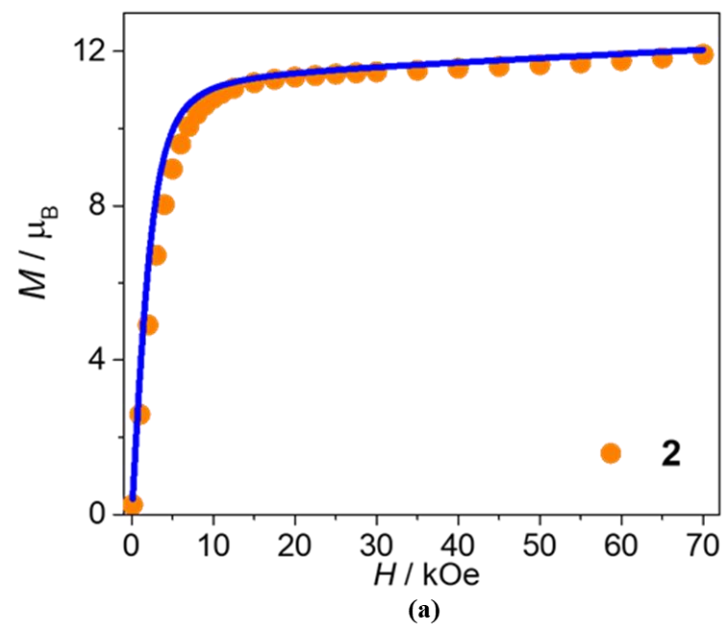
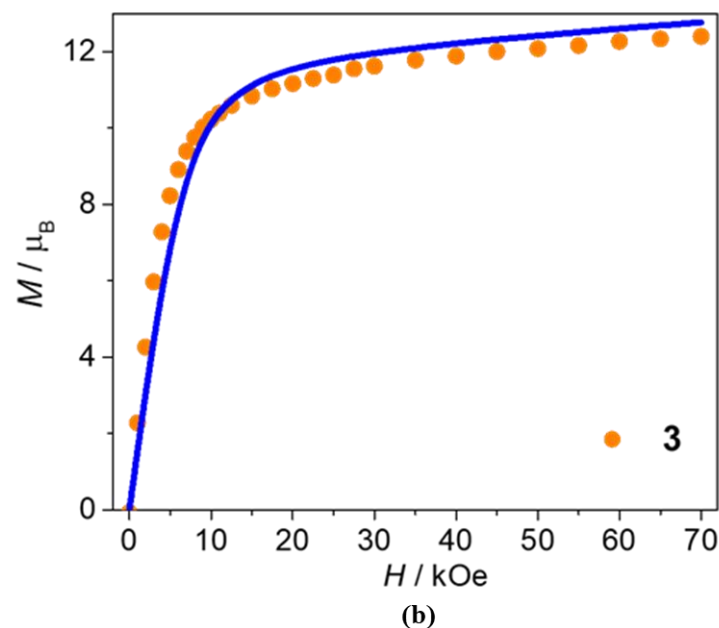


Figure S12. Thermal dependence of the molecular magnetic susceptibility for (a) monomer complex **1**; (b) dimer complex **2**; (c) dimer complex **3**. The grey diamond boxes are the experimental values, while the solid red lines represent the POLY_ANISO simulated data. NOTE: We have increased the simulated data by 4% to meet the experimental values in **2** and **3** respectively.



(a)



(b)

Figure S13. Magnetization at 2K for (a) dimer complex **2**; (b) dimer complex **3** respectively. Solid blue lines represent the POLY_ANISO simulated data. NOTE: We have increased the simulated data by 4% to meet the experimental values.

Table S19. Exchange and dipolar interaction obtained from the POLY_ANISO simulation from the best fit using the Lines model for complexes **2** and **3**.

Complex	J_{total}	J_{ex}	J_{dipo}	zJ
2 {Dy2}	0.03	0.2	-0.17	-0.005
3 {Dy2}	-0.22	-0.3	0.08	-0.002

Table S20. Energies of the low-lying non-Kramers' exchange doublets along with g_{zz} and tunneling gap obtained from POLY_ANISO simulation of complex **2**.

Exchange doublets	Energy/cm ⁻¹	g_{zz}	Δ_{tunnel}
1	0.0	39.3429	7.46E-06
2	2.2	0.0058	1.12E-05
3	99.8	36.1204	9.54E-05
4	99.9	36.1210	5.51E-05
5	101.4	2.8498	8.76E-05
6	101.4	2.8369	6.52E-05
7	199.6	33.0957	6.80E-04
8	200.7	0.01209	8.53E-04

Table S21. Energies of the low-lying non-Kramers' exchange doublets along with g_{zz} and tunneling gap obtained from POLY_ANISO simulation of complex **3**.

Exchange doublets	Energy/cm ⁻¹	g_{zz}	Δ_{tunnel}
1	0.0	17.8358	5.34E-05
2	2.2	34.2640	5.50E-05
3	52.0	18.5109	2.19E-05
4	53.7	32.0144	2.11E-05
5	94.4	8.0127	1.04E-04
6	97.6	36.1903	1.04E-04
7	146.3	7.9437	3.58E-05
8	149.1	34.1280	2.87E-05

Table S22. BS-DFT computed energies of high-spin and broken-symmetry solution of Gd analogue of complex **1** using $H=-JS_1S_2$ formalism. All J values are provided in cm⁻¹.

Complex	Solution	Energy (E _h)	$\rho_{\text{Gd1}}, \rho_{\text{Gd2}}$	$\langle S^{**2} \rangle$	J_{GdGd}	$J_{\text{Dy-Dy}} [(49/25) * J_{\text{Gd-Gd}}]$
1	HS	-31222.110262953120	7.0224	56.0123	0.004	0.008
			7.0224			
	BS	-31222.110262656002	7.0224	7.0123		
			-7.0223			

The calculated ferromagnetic intermolecular interaction explains why the single-ion computed $\chi_M T$ vs T. and experimental $\chi_M T$ vs T. data deviates at low temperature (see Figure S11a).

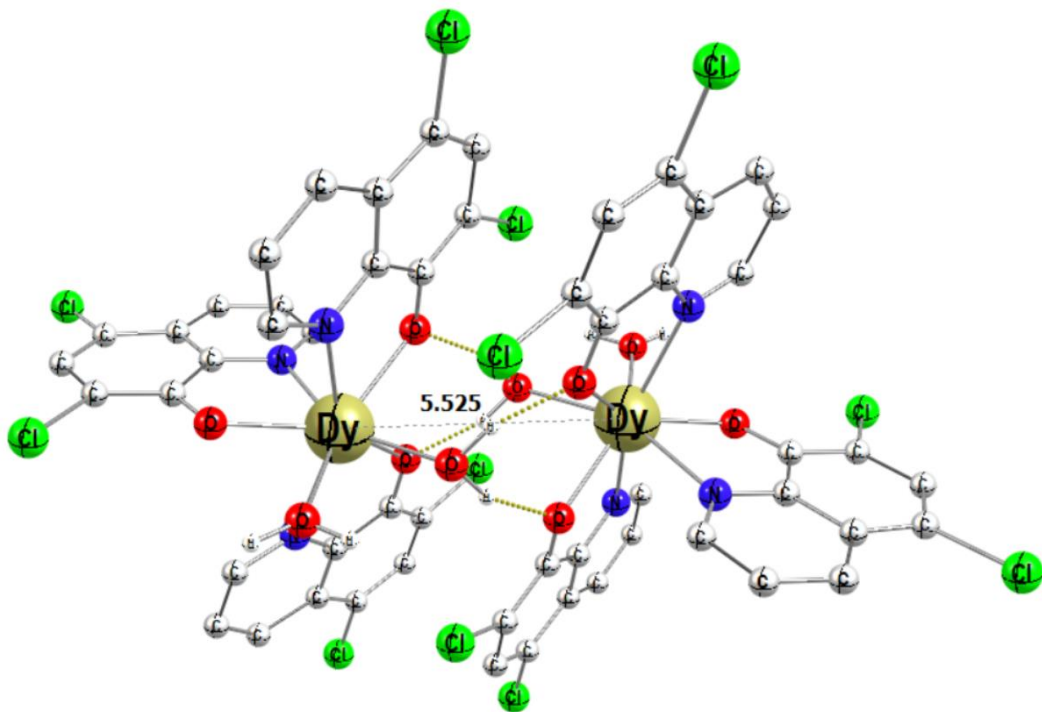


Figure S14. Dimeric structure obtained from the crystal structure of complex **1** to compute the intermolecular exchange interaction.

Table S23. Basis functions used in ab initio CASSCF calculations using MOLCAS code.

Atoms	ANO-RCC basis functions
H	2s.
C	3s2p.
N, O	3s2p.
Cl	4s3p.
Dy	7s6p4d2f1g.

Table S24. Hydrogen optimized cartesian coordinates of complexes **1-3**.

	Complex 1		
Dy	0.000000000000	0.000000000000	0.000000000000
Cl	-4.006300000000	1.264600000000	-3.258600000000
Cl	0.294000000000	-1.296700000000	5.141900000000
Cl	0.127000000000	-2.921100000000	-4.484700000000
Cl	-6.015100000000	4.267000000000	0.723000000000
Cl	-3.865500000000	-4.578200000000	4.241100000000
Cl	4.800100000000	-4.897800000000	-2.764100000000
O	-1.736300000000	0.761100000000	-1.335300000000
O	0.103000000000	-0.722900000000	2.188700000000
O	1.271100000000	1.321800000000	-1.529900000000
O	0.150400000000	-1.393500000000	-1.893600000000
O	1.444500000000	1.486300000000	1.229300000000
N	-1.617300000000	-1.839000000000	0.483600000000
N	-1.648700000000	1.548100000000	1.200100000000
N	2.030000000000	-1.493200000000	-0.022300000000
C	-0.745200000000	-1.587800000000	2.670200000000
C	-2.699800000000	1.550300000000	-0.908500000000
C	1.163700000000	-2.191000000000	-2.099800000000
C	-0.831800000000	-1.977700000000	3.997700000000
C	-3.799100000000	1.935300000000	-1.657800000000
C	-2.676900000000	2.011500000000	0.447700000000
C	-3.693100000000	2.847000000000	0.981400000000
C	-2.653400000000	-3.168300000000	2.240600000000
C	-1.697500000000	-2.221300000000	1.788000000000
C	2.191900000000	-2.278300000000	-1.122500000000
C	1.334200000000	-2.972300000000	-3.224900000000
C	-3.520700000000	-3.706200000000	1.261700000000
C	-3.397500000000	-3.320100000000	-0.034000000000
C	-1.595700000000	1.893900000000	2.477900000000
C	-3.582800000000	3.198100000000	2.347700000000
C	-4.809900000000	2.772800000000	-1.161600000000
C	-2.438200000000	-2.390400000000	-0.388500000000
C	-1.768300000000	-2.906100000000	4.476800000000
C	2.948300000000	-1.520700000000	0.921200000000
C	3.327100000000	-3.118900000000	-1.271900000000
C	-4.747300000000	3.228700000000	0.122500000000
C	-2.554600000000	2.738400000000	3.075800000000
C	-2.660200000000	-3.476200000000	3.624200000000
C	2.444500000000	-3.807100000000	-3.426800000000
C	4.278900000000	-3.115000000000	-0.240500000000
C	4.092200000000	-2.331800000000	0.846800000000
C	3.405900000000	-3.886800000000	-2.480300000000
H	2.204500000000	1.482300000000	-1.766700000000
H	0.819600000000	1.136000000000	-2.384000000000
H	1.507400000000	2.449700000000	1.368900000000

H	1.312700000000	1.089700000000	2.123800000000
H	-4.279200000000	-4.438300000000	1.577900000000
H	-4.056300000000	-3.735700000000	-0.811100000000
H	-0.789100000000	1.443200000000	3.082100000000
H	-4.360600000000	3.843400000000	2.784200000000
H	-5.652700000000	3.042800000000	-1.811900000000
H	-2.313800000000	-2.062600000000	-1.434900000000
H	-1.779900000000	-3.154000000000	5.546600000000
H	2.766000000000	-0.898300000000	1.813300000000
H	-2.454500000000	2.984000000000	4.144200000000
H	2.517400000000	-4.389900000000	-4.354800000000
H	5.163300000000	-3.763300000000	-0.340300000000
H	4.818400000000	-2.317400000000	1.673300000000
Complex 2			
Dy	0.000000000000	0.000000000000	0.000000000000
Dy	0.205900000000	-0.873300000000	-3.774100000000
Cl	-0.369000000000	3.509700000000	3.816900000000
Cl	3.253700000000	0.690400000000	6.638800000000
Cl	1.552500000000	-4.997700000000	-0.015700000000
Cl	-2.534000000000	-6.093700000000	3.316300000000
Cl	-3.056000000000	-1.808900000000	-3.965000000000
Cl	-6.295000000000	2.380300000000	-3.114100000000
Cl	0.575000000000	-4.383000000000	-7.591000000000
Cl	-3.047800000000	-1.563700000000	-10.412900000000
Cl	-1.346600000000	4.124500000000	-3.758400000000
Cl	2.740000000000	5.220400000000	-7.090400000000
Cl	3.261900000000	0.935600000000	0.190900000000
Cl	6.500900000000	-3.253600000000	-0.660000000000
O	-0.032300000000	1.378900000000	1.776400000000
O	0.295000000000	-2.286300000000	-0.160700000000
O	-1.287700000000	-0.476500000000	-1.917200000000
O	0.456300000000	2.053800000000	-1.101500000000
O	0.238200000000	-2.252100000000	-5.550500000000
O	-0.089100000000	1.413000000000	-3.613400000000
O	1.493700000000	-0.396800000000	-1.856900000000
O	-0.250400000000	-2.927100000000	-2.672600000000
N	1.493500000000	-0.801400000000	1.992100000000
N	-1.670600000000	-1.379300000000	1.378000000000
N	-2.141400000000	1.411400000000	-0.192000000000
N	-1.287600000000	-0.071900000000	-5.766200000000
N	1.876500000000	0.506000000000	-5.152000000000
N	2.347300000000	-2.284700000000	-3.582000000000
C	0.687700000000	2.120600000000	3.921600000000
C	1.478000000000	1.958600000000	5.066400000000
C	2.270100000000	0.899700000000	5.210800000000
C	2.401500000000	-0.092800000000	4.169200000000
C	1.538400000000	0.092200000000	3.018200000000
C	0.694100000000	1.256900000000	2.866300000000
C	3.159500000000	-1.214700000000	4.191700000000

C	3.1793000000000	-2.1194000000000	3.1218000000000
C	2.2996000000000	-1.8778000000000	2.0463000000000
C	-0.2693000000000	-3.1242000000000	0.6581000000000
C	0.1119000000000	-4.4528000000000	0.8216000000000
C	-0.5695000000000	-5.3426000000000	1.6500000000000
C	-1.6593000000000	-4.9578000000000	2.3381000000000
C	-2.0800000000000	-3.5775000000000	2.3050000000000
C	-1.3626000000000	-2.6917000000000	1.4779000000000
C	-3.1918000000000	-3.1147000000000	3.0089000000000
C	-3.4695000000000	-1.7245000000000	2.9041000000000
C	-2.6790000000000	-0.9288000000000	2.0906000000000
C	-2.5034000000000	0.0920000000000	-2.1169000000000
C	-3.3439000000000	-0.3397000000000	-3.0810000000000
C	-4.5648000000000	0.3701000000000	-3.3808000000000
C	-4.8625000000000	1.5094000000000	-2.6808000000000
C	-4.0761000000000	1.9134000000000	-1.5753000000000
C	-4.3484000000000	2.9892000000000	-0.7400000000000
C	-3.5716000000000	3.2290000000000	0.3290000000000
C	-2.4760000000000	2.4583000000000	0.6017000000000
C	-2.8706000000000	1.1398000000000	-1.2963000000000
C	0.5367000000000	3.4294000000000	-0.7279000000000
C	-0.4818000000000	-2.9939000000000	-7.6957000000000
C	-1.2721000000000	-2.8318000000000	-8.8405000000000
C	-2.0641000000000	-1.7730000000000	-8.9849000000000
C	-2.1955000000000	-0.7804000000000	-7.9433000000000
C	-1.3325000000000	-0.9655000000000	-6.7923000000000
C	-0.4882000000000	-2.1302000000000	-6.6404000000000
C	-2.9536000000000	0.3414000000000	-7.9658000000000
C	-2.9734000000000	1.2461000000000	-6.8959000000000
C	-2.0937000000000	1.0045000000000	-5.8204000000000
C	0.4752000000000	2.2509000000000	-4.4322000000000
C	0.0940000000000	3.5795000000000	-4.5956000000000
C	0.7754000000000	4.4694000000000	-5.4241000000000
C	1.8652000000000	4.0845000000000	-6.1122000000000
C	2.2859000000000	2.7042000000000	-6.0791000000000
C	1.5685000000000	1.8185000000000	-5.2520000000000
C	3.3978000000000	2.2414000000000	-6.7830000000000
C	3.6755000000000	0.8512000000000	-6.6782000000000
C	2.8850000000000	0.0555000000000	-5.8647000000000
C	2.7093000000000	-0.9653000000000	-1.6572000000000
C	3.5499000000000	-0.5336000000000	-0.6930000000000
C	4.7707000000000	-1.2434000000000	-0.3933000000000
C	5.0684000000000	-2.3827000000000	-1.0932000000000
C	4.2820000000000	-2.7866000000000	-2.1988000000000
C	4.5543000000000	-3.8624000000000	-3.0341000000000
C	3.7775000000000	-4.1023000000000	-4.1031000000000
C	2.6819000000000	-3.3316000000000	-4.3758000000000
C	3.0765000000000	-2.0131000000000	-2.4778000000000
C	-0.3308000000000	-4.3027000000000	-3.0462000000000
H	1.4085000000000	2.7135000000000	5.8622000000000

H	3.802600000000	-1.400100000000	5.067800000000
H	3.821100000000	-3.010800000000	3.132200000000
H	2.248800000000	-2.564900000000	1.187600000000
H	-0.214300000000	-6.381500000000	1.709500000000
H	-3.795100000000	-3.789800000000	3.630400000000
H	-4.313700000000	-1.280400000000	3.451700000000
H	-2.893100000000	0.149800000000	2.008600000000
H	-5.215700000000	0.010600000000	-4.188100000000
H	-5.236400000000	3.604900000000	-0.951700000000
H	-3.803100000000	4.071900000000	1.000300000000
H	-1.822500000000	2.607600000000	1.476400000000
H	-0.434700000000	3.853100000000	-0.371100000000
H	0.890300000000	4.045300000000	-1.594100000000
H	1.302300000000	3.571200000000	0.076100000000
H	-1.202600000000	-3.586800000000	-9.636300000000
H	-3.596700000000	0.526800000000	-8.841900000000
H	-3.615100000000	2.137500000000	-6.906300000000
H	-2.042900000000	1.691600000000	-4.961700000000
H	0.420200000000	5.508200000000	-5.483600000000
H	4.001100000000	2.916500000000	-7.404500000000
H	4.519600000000	0.407100000000	-7.225800000000
H	3.099000000000	-1.023100000000	-5.782700000000
H	5.421600000000	-0.883900000000	0.414000000000
H	5.442300000000	-4.478200000000	-2.822400000000
H	4.009000000000	-4.945200000000	-4.774300000000
H	2.028400000000	-3.480900000000	-5.250500000000
H	0.640700000000	-4.726400000000	-3.402900000000
H	-0.684400000000	-4.918600000000	-2.180000000000
H	-1.096300000000	-4.444500000000	-3.850200000000
Complex 3			
Dy	0.000000000000	0.000100000000	0.000100000000
Dy	-4.040800000000	0.776600000000	0.031900000000
Cl	0.426000000000	-3.383500000000	-3.916000000000
Cl	5.745800000000	-3.243700000000	-3.052700000000
Cl	-0.251400000000	-5.676100000000	4.742900000000
Cl	1.703300000000	-0.673700000000	4.940400000000
Cl	2.177900000000	7.107300000000	0.256800000000
Cl	0.109400000000	3.906700000000	-3.528900000000
Cl	-5.893300000000	-4.743700000000	-4.463900000000
Cl	-4.772100000000	-4.354000000000	0.778900000000
Cl	-9.302000000000	4.019400000000	3.982200000000
Cl	-4.950700000000	1.076700000000	5.181600000000
Cl	-1.458000000000	7.659800000000	-0.384200000000
Cl	-3.894000000000	4.301200000000	-3.835700000000
O	0.812900000000	-0.562100000000	2.069800000000
O	0.365500000000	-1.218200000000	-1.866000000000
O	0.096400000000	1.836800000000	-1.337600000000
O	-3.973600000000	2.440500000000	-1.505900000000
O	-4.672900000000	0.831600000000	2.218400000000

O	-4.6668000000000	-1.3859000000000	0.2144000000000
O	-2.0590000000000	0.0543000000000	1.3015000000000
O	-2.1186000000000	0.0001000000000	-1.2534000000000
N	-0.2767000000000	-2.5403000000000	0.6853000000000
N	2.4424000000000	-0.2026000000000	-0.5035000000000
N	0.8441000000000	2.1507000000000	1.1807000000000
N	-3.0102000000000	2.9124000000000	0.9385000000000
N	-6.2220000000000	1.9870000000000	0.3826000000000
N	-5.1200000000000	-0.1884000000000	-2.0995000000000
N	-2.1918000000000	-0.5208000000000	2.5018000000000
N	-2.1185000000000	0.0001000000000	-2.5995000000000
C	0.6790000000000	-1.6829000000000	2.6377000000000
C	1.0247000000000	-1.9703000000000	3.9955000000000
C	0.7808000000000	-3.1778000000000	4.6188000000000
C	0.1570000000000	-4.2109000000000	3.8959000000000
C	-0.1826000000000	-4.0533000000000	2.5906000000000
C	0.0656000000000	-2.7710000000000	1.9824000000000
C	-0.8361000000000	-3.4947000000000	-0.0536000000000
C	-1.1223000000000	-4.7751000000000	0.4224000000000
C	-0.7998000000000	-5.0547000000000	1.7695000000000
C	3.4599000000000	0.3305000000000	0.1384000000000
C	4.8009000000000	0.0192000000000	-0.1301000000000
C	5.0558000000000	-0.9819000000000	-1.0656000000000
C	4.0203000000000	-1.5977000000000	-1.7620000000000
C	2.6905000000000	-1.1632000000000	-1.4772000000000
C	1.5424000000000	-1.6887000000000	-2.1490000000000
C	1.7584000000000	-2.6894000000000	-3.0843000000000
C	3.0824000000000	-3.1715000000000	-3.3297000000000
C	4.1429000000000	-2.6582000000000	-2.7324000000000
C	0.5278000000000	2.9612000000000	-1.0309000000000
C	0.6194000000000	4.0710000000000	-1.9103000000000
C	1.1433000000000	5.3155000000000	-1.5221000000000
C	1.5277000000000	5.5421000000000	-0.1884000000000
C	1.4640000000000	4.4959000000000	0.7565000000000
C	0.9490000000000	3.2567000000000	0.2884000000000
C	1.8088000000000	4.6457000000000	2.0625000000000
C	1.6684000000000	3.5332000000000	3.0217000000000
C	1.2349000000000	2.3340000000000	2.4465000000000
C	-1.6652000000000	0.0539000000000	3.6091000000000
C	-1.8065000000000	-0.5345000000000	4.8216000000000
C	-2.4755000000000	-1.7606000000000	4.9689000000000
C	-2.8465000000000	-1.6841000000000	2.5863000000000
C	-3.0045000000000	-2.3179000000000	3.8011000000000
C	-2.2270000000000	-1.1605000000000	-3.2247000000000
C	-2.2959000000000	-1.2336000000000	-4.6014000000000
C	-2.2671000000000	-0.0530000000000	-5.3421000000000
C	-2.1127000000000	1.1319000000000	-4.6747000000000
C	-2.0468000000000	1.1627000000000	-3.2856000000000
C	-5.3564000000000	0.4303000000000	-3.2500000000000
C	-5.7394000000000	-0.2654000000000	-4.4478000000000

C	-5.810200000000	-1.637100000000	-4.408600000000
C	-5.536700000000	-2.334600000000	-3.219700000000
C	-5.226700000000	-1.564600000000	-2.070400000000
C	-4.958700000000	-2.167100000000	-0.779800000000
C	-5.034500000000	-3.545900000000	-0.748500000000
C	-5.334900000000	-4.322400000000	-1.866500000000
C	-5.556800000000	-3.737100000000	-3.062300000000
C	-6.971700000000	2.549100000000	-0.558900000000
C	-8.142200000000	3.270900000000	-0.276500000000
C	-8.488600000000	3.461200000000	1.049000000000
C	-7.707500000000	2.920400000000	2.067100000000
C	-7.942600000000	3.086000000000	3.459500000000
C	-7.113300000000	2.525900000000	4.390600000000
C	-5.972800000000	1.778300000000	3.980800000000
C	-5.688600000000	1.547900000000	2.642000000000
C	-6.566900000000	2.150100000000	1.685700000000
C	-2.597100000000	3.138100000000	2.167700000000
C	-1.931800000000	4.325800000000	2.546800000000
C	-1.772900000000	5.338000000000	1.607100000000
C	-2.879600000000	3.906100000000	0.000900000000
C	-2.251400000000	5.140100000000	0.306600000000
C	-2.173900000000	6.108500000000	-0.742400000000
C	-2.672800000000	5.844800000000	-1.953100000000
C	-3.270100000000	4.594800000000	-2.233800000000
C	-3.421500000000	3.605400000000	-1.285300000000
H	1.043500000000	-3.324200000000	5.674400000000
H	-1.025700000000	-3.226500000000	-1.107000000000
H	-1.582600000000	-5.535400000000	-0.222700000000
H	-1.005500000000	-6.041000000000	2.209900000000
H	3.208800000000	1.071000000000	0.916400000000
H	5.613400000000	0.515200000000	0.417500000000
H	6.089900000000	-1.294100000000	-1.279000000000
H	3.202900000000	-3.986200000000	-4.059700000000
H	1.211400000000	6.130000000000	-2.255400000000
H	2.185800000000	5.619800000000	2.409200000000
H	1.954400000000	3.623600000000	4.076500000000
H	1.183300000000	1.416800000000	3.061600000000
H	-1.122200000000	0.988700000000	3.437500000000
H	-1.354300000000	-0.035400000000	5.690100000000
H	-3.305800000000	-2.041600000000	1.651000000000
H	-3.555500000000	-3.268200000000	3.814100000000
H	-2.262100000000	-2.038900000000	-2.571500000000
H	-2.393700000000	-2.219300000000	-5.074600000000
H	-2.061100000000	2.096600000000	-5.197800000000
H	-1.892900000000	2.065800000000	-2.694600000000
H	-5.211000000000	1.525100000000	-3.245400000000
H	-5.947800000000	0.302500000000	-5.365600000000
H	-6.080600000000	-2.216900000000	-5.304700000000
H	-5.378200000000	-5.415700000000	-1.764800000000
H	-6.625600000000	2.421600000000	-1.596900000000

H	-8.742000000000	3.695900000000	-1.093400000000
H	-9.383400000000	4.042100000000	1.321000000000
H	-7.307500000000	2.661600000000	5.463400000000
H	-2.809300000000	2.344800000000	2.902900000000
H	-1.583100000000	4.452600000000	3.581500000000
H	-1.278400000000	6.286500000000	1.861300000000
H	-2.617400000000	6.591400000000	-2.758000000000
H	-2.581900000000	-2.247100000000	5.947600000000
H	-2.336600000000	-0.080000000000	-6.440200000000

References

- S1) SAINT Software Users Guide, version 7.0; Bruker Analytical X-Ray Systems: Madison, WI, 1999.
- S2) G. M. Sheldrick, SADABS, version 2.03; Bruker Analytical X-Ray Systems, Madison, WI, 2000.
- S3) G. M. Sheldrick, SHELXTL, Version 6.14, Bruker AXS, Inc.; Madison, WI 2000-2003.
- S4) Dolomanov, O. V.; Bourhis, L. J.; Gildea, R. J.; Howard, J. A. K.; Puschmann, H. OLEX2: A Complete Structure Solution, Refinement and Analysis Program. *J. Appl. Crystallogr.* **2009**, 42, 339–341.
- S5) Neese, F. Software Update: The ORCA Program System—Version 5.0. *WIREs Computational Molecular Science* n/a (n/a), e1606.
- S6) Becke, A. D. Density-Functional Exchange-Energy Approximation with Correct Asymptotic Behavior. *Phys. Rev. A* **1988**, 38, 3098–3100.
- S7) Perdew, J. P. Density-Functional Approximation for the Correlation Energy of the Inhomogeneous Electron Gas. *Phys. Rev. B* **1986**, 33, 8822–8824.
- S8) Weigend, F.; Ahlrichs, R. Balanced Basis Sets of Split Valence, Triple Zeta Valence and Quadruple Zeta Valence Quality for H to Rn: Design and Assessment of Accuracy. *Phys. Chem. Chem. Phys.* **2005**, 7, 3297–3305.
- S9) Weigend, F. Accurate Coulomb-Fitting Basis Sets for H to Rn. *Phys. Chem. Chem. Phys.* **2006**, 8, 1057–1065.
- S10) Aquilante, F.; Autschbach, J.; Carlson, R. K.; Chibotaru, L. F.; Delcey, M. G.; De Vico, L.; Fdez. Galván, I.; Ferré, N.; Frutos, L. M.; Gagliardi, L.; Garavelli, M.; Giussani, A.; Hoyer, C. E.; Li Manni, G.; Lischka, H.; Ma, D.; Malmqvist, P. Å.; Müller, T.; Nenov, A.; Olivucci, M.; Pedersen, T. B.; Peng, D.; Plasser, F.; Pritchard, B.; Reiher, M.; Rivalta, I.; Schapiro, I.; Segarra-Martí, J.; Stenrup, M.; Truhlar, D. G.; Ungur, L.; Valentini, A.; Vancoillie, S.; Veryazov, V.; Vysotskiy, V. P.; Weingart, O.; Zapata, F.; Lindh, R. Molcas 8: New Capabilities for Multiconfigurational Quantum Chemical Calculations across the Periodic Table. *Journal of Computational Chemistry* **2016**, 37, 506–541.
- S11) Roos, B. O.; Taylor, P. R.; Sigbahn, P. E. M. A Complete Active Space SCF Method (CASSCF) Using a Density Matrix Formulated Super-CI Approach. *Chemical Physics* **1980**, 48, 157–173.
- S12) Roos, B. O.; Veryazov, V.; Widmark, P.-O. Relativistic Atomic Natural Orbital Type Basis Sets for the Alkaline and Alkaline-Earth Atoms Applied to the Ground-State Potentials for the

- Corresponding Dimers. *Theor Chem Acc* **2004**, *111*, 345–351.
- S13) Roos, B. O.; Lindh, R.; Malmqvist, P.-Å.; Veryazov, V.; Widmark, P.-O.; Borin, A. C. New Relativistic Atomic Natural Orbital Basis Sets for Lanthanide Atoms with Applications to the Ce Diatom and LuF₃. *J. Phys. Chem. A* **2008**, *112*, 11431–11435.
- S14) Aquilante, F.; Lindh, R.; Bondo Pedersen, T. Unbiased Auxiliary Basis Sets for Accurate Two-Electron Integral Approximations. *J. Chem. Phys.* **2007**, *127*, 114107.
- S15) Malmqvist, P. Å.; Roos, B. O.; Schimmelpfennig, B. The Restricted Active Space (RAS) State Interaction Approach with Spin–Orbit Coupling. *Chemical Physics Letters* **2002**, *357*, 230–240.
- S16) Chibotaru, L. F.; Ungur, L. Ab Initio Calculation of Anisotropic Magnetic Properties of Complexes. I. Unique Definition of Pseudospin Hamiltonians and Their Derivation. *J. Chem. Phys.* **2012**, *137*, 064112.
- S17) Tian, H.; Ungur, L.; Zhao, L.; Ding, S.; Tang, J.; Chibotaru, L. F. Exchange Interactions Switch Tunneling: A Comparative Experimental and Theoretical Study on Relaxation Dynamics by Targeted Metal Ion Replacement. *Chem. Eur. J.* **2018**, *24*, 9928–9939.
- S18) Chibotaru, L. F.; Ungur, L.; Aronica, C.; Elmoll, H.; Pilet, G.; Luneau, D. Structure, Magnetism, and Theoretical Study of a Mixed-Valence CoII₃CoIII₄ Heptanuclear Wheel: Lack of SMM Behavior despite Negative Magnetic Anisotropy. *J. Am. Chem. Soc.* **2008**, *130*, 12445–12455.
- S19) Chibotaru, L. F.; Ungur, L.; Soncini, A. The Origin of Nonmagnetic Kramers Doublets in the Ground State of Dysprosium Triangles: Evidence for a Toroidal Magnetic Moment. *Angew. Chem. Int. Ed. Edition* **2008**, *47*, 4126–4129.